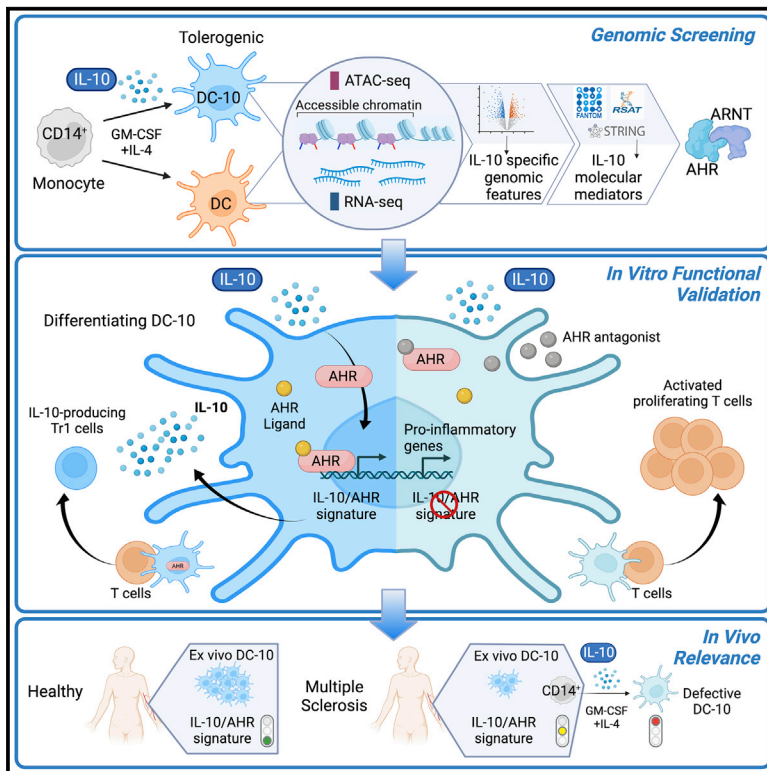**Article**

Aryl hydrocarbon receptor activity downstream of IL-10 signaling is required to promote regulatory functions in human dendritic cells

Graphical abstract

Authors

Daniele Avancini, Alessandro Testori, Lucia Fresolone, ..., Vittorio Martinelli, Francesca R. Santoni de Sio, Silvia Gregori

Correspondence

gregori.silvia@hsr.it

In brief

Avancini et al. investigate IL-10-mediated induction of human tolerogenic dendritic cells (tolDCs) and identify AHR as a key player for establishing genomic and tolerogenic features. They find the IL-10/AHR genomic signature active in circulating healthy tolDCs and altered in multiple sclerosis patients' IL-10-induced, functionally defective tolDCs.

Highlights

- IL-10 imprints chromatin and transcriptome in monocyte-derived tolDCs

- AHR activity is needed downstream of IL-10 to establish IL-10 induced core genes

- IL-10/AHR genomic signature is evident *in vivo* in healthy tolDCs

- MS patients show alterations in IL-10/AHR genomic signature and tolDCs

CellPress

Article

Aryl hydrocarbon receptor activity downstream of IL-10 signaling is required to promote regulatory functions in human dendritic cells

Daniele Avancini,[1] Alessandro Testori,[1] Lucia Fresolone,[1] Grazia Andolfi,[1] Michela Vuono,[1] Vittorio Martinelli,[2] Francesca R. Santoni de Sio,[1,3] and Silvia Gregori[1,3,4,*]

[1]San Raffaele Telethon Institute for Gene Therapy (SR-TIGET), IRCCS San Raffaele Scientific Institute, 20132 Milan, Italy
[2]Neurology Unit, IRCCS San Raffaele Scientific Institute, 20132 Milan, Italy
[3]Senior author
[4]Lead contact
*Correspondence: gregori.silvia@hsr.it
https://doi.org/10.1016/j.celrep.2023.112193

SUMMARY

Interleukin (IL)-10 is a main player in peripheral immune tolerance, the physiological mechanism preventing immune reactions to self/harmless antigens. Here, we investigate IL-10-induced molecular mechanisms generating tolerogenic dendritic cells (tolDC) from monocytes. Using genomic studies, we show that IL-10 induces a pattern of accessible enhancers exploited by aryl hydrocarbon receptor (AHR) to promote expression of a set of core genes. We demonstrate that AHR activity occurs downstream of IL-10 signaling in myeloid cells and is required for the induction of tolerogenic activities in DC. Analyses of circulating DCs show that IL-10/AHR genomic signature is active *in vivo* in health. In multiple sclerosis patients, we instead observe significantly altered signature correlating with functional defects and reduced frequencies of IL-10-induced-tolDC *in vitro* and *in vivo*. Our studies identify molecular mechanisms controlling tolerogenic activities in human myeloid cells and may help in designing therapies to re-establish immune tolerance.

INTRODUCTION

Peripheral immune tolerance is maintained by regulatory cells, immune subsets that control effector responses. T regulatory cells (Tregs) have long been recognized and studied, while antigen-presenting regulatory cells were more recently identified. Therefore, while the molecular mechanisms and gene expression patterns defining the identity and function of Tregs have been deeply studied, the molecular patterns driving tolerogenic activities in antigen-presenting cells (APCs) remain less defined.[1]

Regulatory cells act via cell-cell contact inhibitory mechanisms and secretion of anti-inflammatory factors. One of the most studied anti-inflammatory cytokines is interleukin-10 (IL-10). Originally identified as a stimulatory cytokine produced by CD4^{+} T helper type 2 (Th2) cells, IL-10's immunosuppressive functions on both APC and T cells have then been established.[2] Accordingly, alterations in IL-10 pathways result in loss of immune tolerance and uncontrolled inflammatory responses leading to human pathologies, such as inflammatory bowel disease and neuroinflammation.[3,4] The canonical IL-10/IL-10 receptor pathway signals through STAT3, which directly alters gene expression to activate the anti-inflammatory program.[2] However, STAT3 can also activate pro-inflammatory genes. The net result of IL-10-mediated gene expression pattern is strictly dependent on the cellular context in which STAT3 is activated, likely relying on the expression of co-factors and the chro-

matin accessibility of target genes and regulatory elements.[5] IL-10 is produced by many immune cells and its expression is regulated by the integration of different stimuli through several pathways.[6] In myeloid cells, IL-10 expression is typically activated downstream of pattern recognition receptors (e.g., TLR), while both TCR and lineage-inducing cytokines can stimulate IL-10 expression in CD4^{+} cells. The transcription factor c-MAF appears to act as a transcriptional activator of IL-10 in myeloid and lymphoid immune cells, while its partner aryl hydrocarbon receptor (AHR) has been described as a key activator of IL-10 gene transcription specifically in T regulatory Type 1 (Tr1) cells.[7]

AHR is a ubiquitously expressed protein, originally identified as an intracellular sensor of environmental pollutants and later recognized as a mediator of numerous cellular processes, including immune responses.[8] AHR resides in the cytoplasm under steady-state conditions. Upon binding to an agonist, AHR binds to its canonical partner AHR Nuclear Translocator (ARNT) and translocates to the nucleus, where it can modulate gene transcription. AHR system is highly complex and can activate different gene patterns depending on its ligand and binding partner(s). Several endogenous/exogenous ligands can act as AHR agonists/antagonists (e.g., tryptophan catabolites, diet derivatives, microbiota metabolites), while several interacting protein partners have been documented (e.g., NF-κB, STATs, epigenetic regulators).[8–10] This implies that the biological result of AHR activation is strictly contextual. Accordingly, in mice,
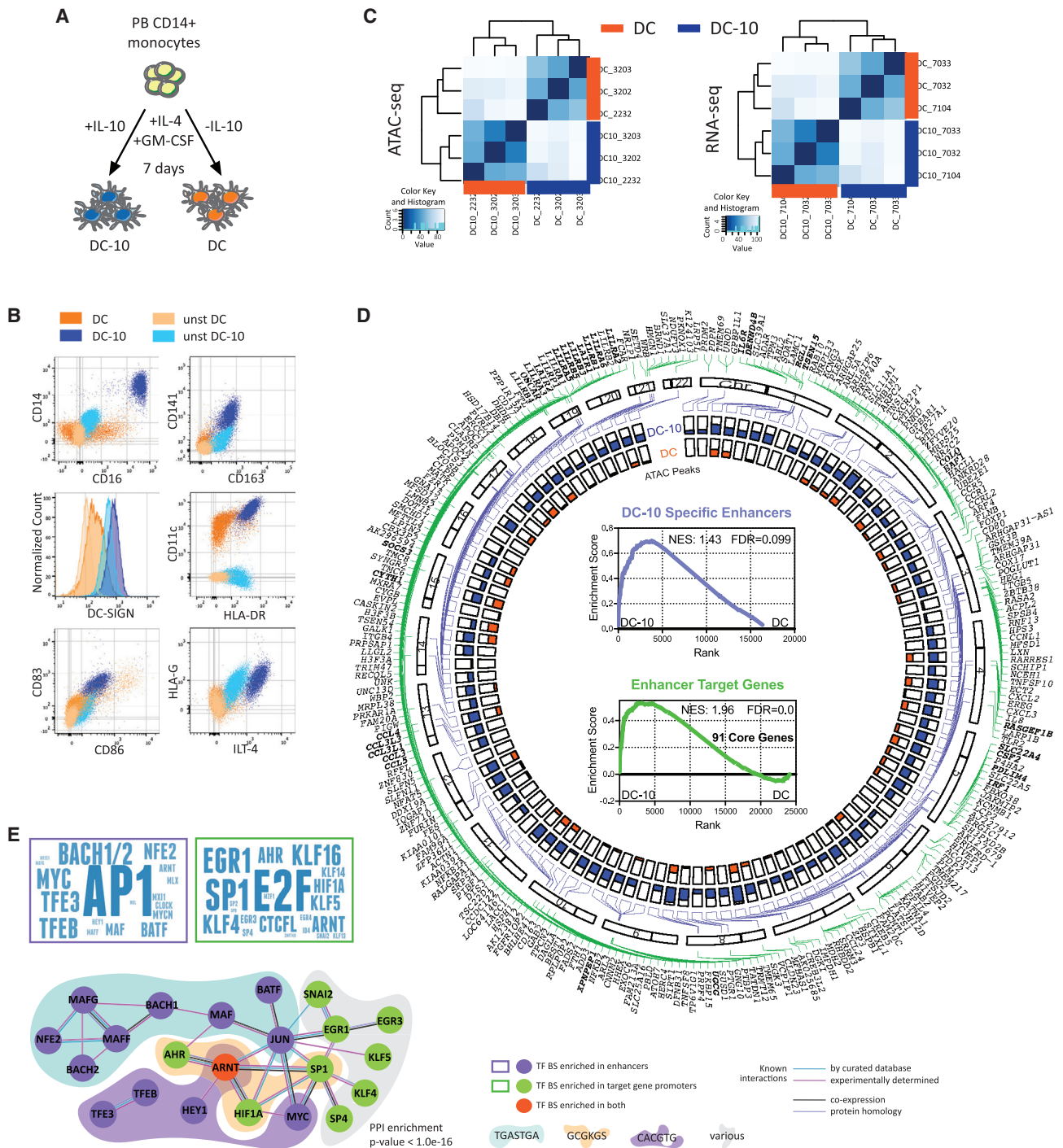
Figure 1. IL-10 impacts chromatin and transcription in DCs

(A) Experimental design. Peripheral blood (PB) CD14+ monocytes were differentiated for 7 days in presence of GM-CSF and IL-4, with (DC-10) or without (DC) IL-10.

(B) Representative plots of DC and DC-10 phenotype by flow cytometry (FC).

(C) Unsupervised clustering heatmaps of ATAC-seq (left) and RNA-seq (right) data from DC and DC-10 from three independent donors.

(D) Circoplot depicting the following: outer layer, location of FANTOM5-identified DC-10-specific enhancers (purple lines), and enhancer target genes (green lines) along chromosomes (bold genes = targets of multiple enhancers); inner layer, ATAC broadpeak maximum value for each enhancer in DC-10s (blue) and DCs (orange). Inner core: GSEA analysis of DC-10-specific enhancers (top, purple) and enhancer target genes (bottom, green) in DC-10 vs. DC transcriptome. Normalized enriched score (NES), false discovery rate (FDR), and number of core genes (bottom) are indicated.

(legend continued on next page)

AHR can induce both inflammatory (Th17) and tolerogenic (Tr1 and Treg) pathways.[8,9] In humans, instead, AHR activity in immune cells has been mainly associated with tolerogenic mechanisms, as described in monocytes, dendritic cells (DCs), CD4^{+} and CD8^{+} T cells, and B cells.[11–15] AHR has also been shown to control human monocyte differentiation into DCs vs. macrophages.[16]

We have previously investigated IL-10-mediated induction of regulatory activity in human myeloid cells. Several protocols have exploited the immunosuppressive abilities of IL-10 to generate tolerogenic (tol)DCs, which can be used as a model system for basic studies and as therapeutic tools to re-establish immune tolerance in human T cell-mediated pathologies. Among them, we have developed an *in vitro* IL-10-based protocol to differentiate tolDCs from human monocytes. These tolDCs, termed DC-10s, can efficiently generate Tr1 cells via secretion of IL-10 and expression of the tolerogenic molecules ILT-4 and HLA-G.[17] We have also identified naturally occurring DC-10s in human peripheral blood, which shares markers, mechanisms of action, and gene transcription patterns with its *in vitro* counterpart and the numbers of which positively correlate with enhanced tolerance.[17–20]

Here, we used DC-10s as a model to assess IL-10-directed chromatin and transcriptome patterns in human tolDC. We found that IL-10 induces a pattern of accessible enhancers, which are exploited by AHR to promote expression of a set of core genes needed for IL-10-mediated induction of tolerogenic activities (e.g., suppression of T cell responses and induction of Tr1 cells) in myeloid cells. IL-10-induced enhancers and core genes were also specifically active in *ex vivo* isolated DC-10s, and their alteration correlated with human autoimmune conditions. This study identifies an IL-10-induced molecular mechanism required for establishing tolerogenic functions in human myeloid cells.

RESULTS

IL-10 alters chromatin accessibility and transcription in human dendritic cells

We investigated the molecular mechanisms underlying IL-10-mediated induction of tolerogenic myeloid cells by using DC-10s as a cellular model in comparison with monocyte-derived DCs (Figure 1A). DC-10s are CD14^{+}CD16^{+}CD141^{+}CD163^{+} and express DC-SIGN, HLA-DR, CD83, and CD86, and the tolerogenic molecules HLA-G and ILT-4 (Figures 1B and S1A).

We used ATAC-seq and RNA-seq to assess chromatin accessibility and transcriptome in DC-10s and DCs differentiated from three independent donors. Following ATAC protocol validation (Figures S1B and S1C), differential analysis revealed that DC-10s and DCs clustered apart and showed thousands of differentially accessible regions and expressed transcripts (Figures 1C and S1D), consistent with the previously described transcriptional profile of DC-10s.[18] Matching results obtained by edgeR

and DESeq2 algorithms identified 1,593 genomic regions as specifically accessible in DC-10s and not in DCs.

By interrogating FANTOM5 human enhancer atlas[21] with the identified DC-10-specific accessible regions, we identified 107 regions defined as robust enhancers that putatively control 268 protein-coding genes (Figure 1D, Table S1). Since active enhancers are actively transcribed and decorated by specific histone marks, we assessed transcription and histone marking of the 107 identified DC-10-specific enhancers.[22,23] Gene set enrichment analysis (GSEA) revealed that DC-10-specific enhancers were transcribed and significantly more expressed in DC-10s as compared with DCs (Figure 1D, inner core, top graph). Identified enhancers were also enriched in H3K4me1 and H3K27ac modifications, validating them as bona fide DC-10 active enhancers (Figure S1E). GSEA confirmed significant enrichment in expression of the 268 protein-coding genes associated with DC-10-specific enhancers in DC-10s compared with DCs, further supporting the relevance of the identified enhancer/target gene network in DC-10s, and allowed us to define the leading-edge subset of 91 target genes as DC-10 core genes (Figure 1D, inner core, bottom graph, Table S2).

To identify transcription factors (TFs) that might control DC-10-specific enhancer and gene activity, we used the regulatory sequence analysis tools (RSAT) peak motifs tool. Enhancer and gene promoter sequences were enriched for binding of pleiotropic (AP1, MYC), Treg-associated (BACH2, MAF/ARNT, BATF, TFEB), and broad-function (E2F, SP/KLF family, EGR)[7,24,25] TFs. Interestingly, we also found enrichment for ARNT complex (AHR/ARNT/HIF1α) binding sites (Figures 1E and S1F). When assessing functional associations using String,[26] we found that TFs putatively binding to DC-10-specific enhancers and promoters were significantly enriched for interactions, when compared with randomly selected TFs, and formed a network around an AHR/ARNT core (Figures 1E and S1G).

These results indicate that IL-10 exposure during monocyte-derived tolDC differentiation prompts the establishment of a specific genomic signature, the activity of which might be controlled by the AHR pathway.

AHR activity regulates IL-10-mediated induction of regulatory functions in DCs

Considering the established roles of AHR in immune tolerance and DC differentiation,[7,16,27–30] we investigated the function of AHR in IL-10-mediated tolDC differentiation and function.

We first verified the activity of the AHR pathway in DC-10s and DCs. In the DC-10 transcriptome, although AHR expression was reduced, the expression of some of its canonical target genes was significantly upregulated as compared with DCs (Figure 2A). However, the AHR functional repressor AHRR was downregulated, suggesting increased AHR activity in DC-10s. We validated by ddPCR differential expression of CYP1B1 and AHRR in DC-10s vs. DCs (Figure 2B). MAF expression was not

---

(E) Transcription factor (TF) binding predictions. Left, word clouds displaying TFs whose binding sites (BSs) were significantly enriched in the 107 DC-10 enhancers (top, purple) and 268 DC-10 enhancer target protein-coding gene promoters (bottom, green); size of TF is proportional to its enrichment score from motif finder analysis. Right, protein-protein interaction network built on TF from word clouds; only connected nodes are shown. Colored clouds identify TFs with shared BSs, with consensus site indicated below. PPI, protein-protein interaction. See Figure S1.
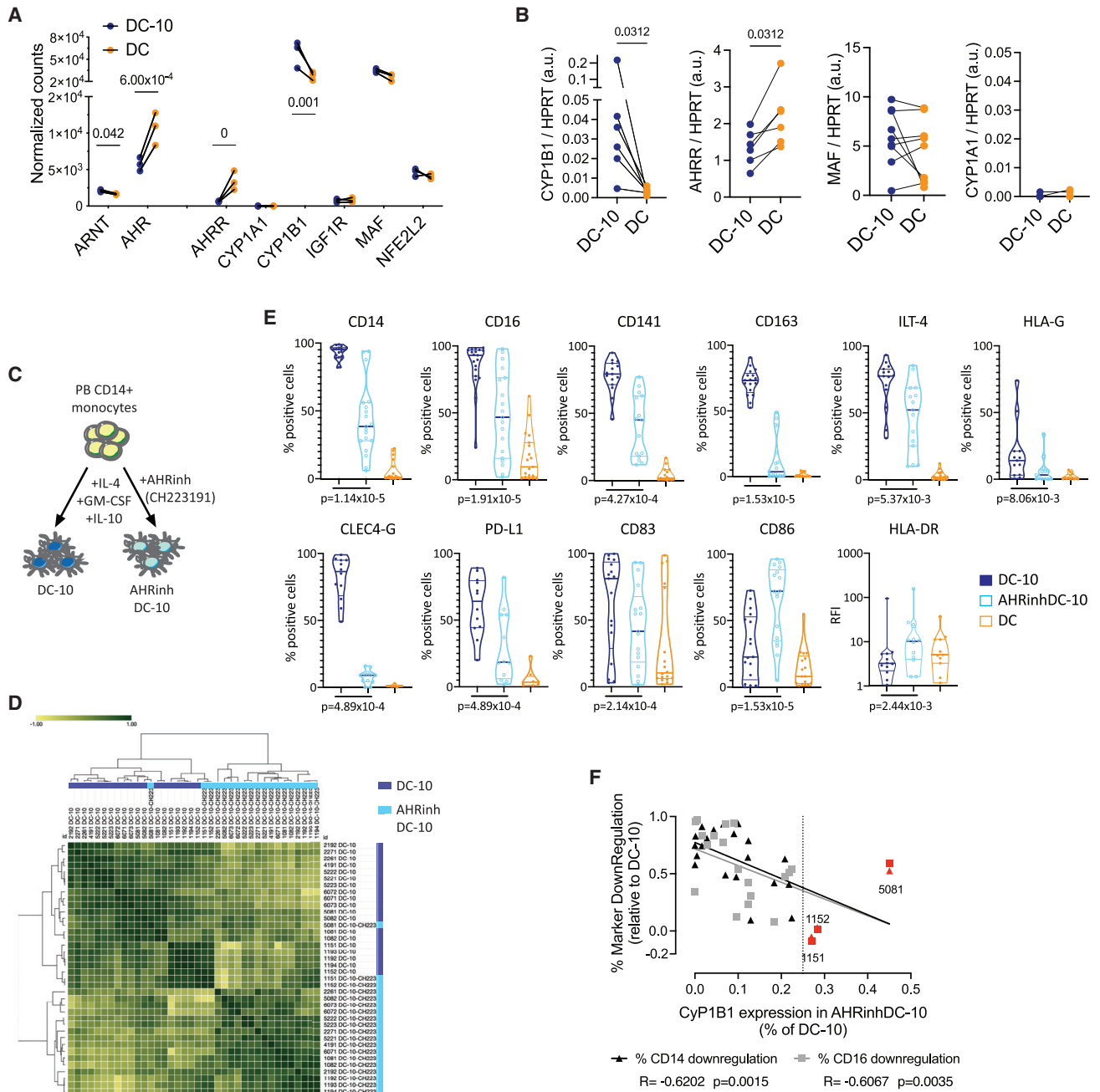
Figure 2. AHR activity characterizes IL-10-induced tolDC

(A) Expression of AHR-related molecules in DC-10s and DCs by RNA-seq; significant false discovery rates (FDRs) are shown.

(B) Expression of AHR targets by ddPCR. The ratio between molecules/μL of the target gene and molecules/μL of the reference HPRT gene is shown in arbitrary units (a.u.). p value by Wilcoxon matched pairs test.

(C) Experimental design. Peripheral blood (PB) CD14^{+} monocytes were differentiated for 7 days in the presence of GM-CSF, IL-4, and IL-10 with (AHRinhDC-10) or without (DC-10) AHR inhibitor CH223191. (D and E) Phenotype of DC-10, AHRinhDC-10, and DC by flow cytometry (FC).

(D) Hierarchical clustering heatmap of DC-10 and AHRinhDC-10 samples based on FC parameters shown in (E).

(E) Violin plots displaying median, interquartile range, and single values of percentages of positive cells or relative fluorescence intensity (RFI) for the indicated markers in DC-10, AHRinhDC-10, and DC samples gated on CD11c^{+} Live/Dead negative population. p values by Wilcoxon matched pairs test (n = 19).

(F) Correlation plot between percentage of CD14 and CD16 downregulation (expressed as 1 − [% positive cells in AHRinhDC-10/% positive cells in donor-matched DC-10]) and CYP1B1 expression in AHRinhDC-10 (% of DC-10) (expressed as normalized CYP1B1 expression in AHRinhDC-10/normalized CYP1B1 expression in DC-10). Linear interpolation, Spearman R and p values are indicated for each marker. Dotted line indicates 25% residual CYP1B1 expression. Samples with a CYP1B1 residual expression >25% are indicated in red. See Figure S2.

differentially expressed, and CYP1A1 was not expressed in either condition (Figures 2A and 2B).

To test whether activation of AHR is required for DC-10 differentiation, we differentiated DC-10s in the presence of the AHR-specific antagonist CH223191 (Figure 2C). AHR-inhibited DC-10 (AHRinhDC-10) yield at the end of differentiation was mildly, although statistically significant, reduced compared with DC-10 (Figure S2A). Consistent with a role for AHR activity downstream of IL-10, AHRinhDC-10s showed a deeply altered phenotype and clustered apart from DC-10s in an unsupervised analysis based on Spearman correlation (Figure 2D). Despite donor variability, AHRinhDC-10s displayed significantly decreased expression of DC-10-specific markers (CD14, CD16, CD141, CD163, and CLEC4G) and the tolerogenic molecules ILT-4, HLA-G, and PD-L1, and an increased expression of CD86 and HLA-DR (Figures 2D, 2E, and S2B). DC differentiation was not affected by AHR inhibition, as indicated by comparable DC-SIGN and CD206 levels in AHRinhDC-10s and DC-10s. CD1a expression, which is very low/negative in DC-10,[17] was further downregulated in AHRinhDC-10s (Figure S2C). The magnitude of the differences in marker expression between DC-10s and AHRinhDC-10s varied among matched samples. To assess whether different levels of AHR inhibition by CH223191 may explain this variability, we measured the expression of CYP1B1 at the end of differentiation in donor-matched samples. In most cases, we CYP1B1 expression in AHRinhDC-10s was below 25% of the expression detected in donor-matched DC-10 (Figure 2F), indicating that CH223191 efficiently antagonized AHR activity.[31,32] CYP1B1 residual expression in AHRinhDC-10s inversely correlated with the extent of DC-10-specific marker downregulation, with the three samples showing >25% CYP1B1 expression clustering together with DC-10 (Figures 2F and 2D). Overall, these results indicate that AHR activity is necessary for the establishment of a tolerogenic phenotype in IL-10-induced DCs.

We then investigated the impact of AHR inhibition on IL-10-induced tolerogenic functions: inhibition of T cell proliferation and induction Tr1 cells[17] (Figures 3A and 3D). Allogeneic CD4+ T cells were stimulated with DCs, mature DCs (mDCs), DC-10s, AHRinhDC-10s, or with DCs or DC-10s in the presence of CH223191. AHRinhDC-10s induced significantly higher T cell proliferation and activation compared with DC-10s, which, as expected, induced T cell hypo-proliferation and hypo-activation (Figures 3B, S3A, and S3B). Consistently, T cells stimulated by AHRinhDC-10s produced significantly higher levels of IFNγ than DC-10-stimulated T cells (Figures 3C and S3C). The observed differences were due to increased stimulation by AHRinhDC-10s and not to a bystander effect from AHR antagonist leftover in culture, as the addition of CH223191 during CD4+ T cell stimulation did not affect proliferation and IFNγ production (Figures 3B, 3C, and S3A–S3C). Increased response to AHRinhDC-10s was observed in both total and naive CD4+ T cells, indicating that AHRinhDC-10s were bona fide DCs and not undifferentiated monocytes, which cannot prime naive T cells (Figures 3B, 3C, and S3B).

We found proliferation and activation of AHRinhDC-10-stimulated T cells significantly higher when compared with DC-10-stimulated T cells also in long-term mixed lymphocyte reaction (MLR) assay (Figures 3D, 3E, and S3D). Meanwhile, the percentage of induced Tr1 cells, assessed by co-expression of LAG-3 and CD49b,[33] was significantly lower (Figure 3E). Moreover, when restimulated with allogeneic DCs generated from the same DC donor used in priming, AHRinhDC-10-primed T cells showed significantly reduced anergic response and IL-10 production, increased activation, and IFNγ production compared with DC-10-primed T cells (Figures 3F and S3E).

Together, these findings indicate that IL-10-induced differentiation of tolDC is severely impaired when AHR activation is abolished.

AHR-induced tolerogenic features are dependent on IL-10 and are abrogated by MTOR pathway activation

AHR activation can modulate human monocyte-derived DCs toward a regulatory phenotype, independently of IL-10.[34,35] We thus investigated if AHR inhibition or activation were able per se to induce a pro-inflammatory or tolerogenic skew, respectively, in monocyte-derived DCs. To test if AHR activation can prompt DC-10-like cell differentiation, we differentiated DCs in the presence of ITE, a non-toxic AHR agonist able to induce human Treg differentiation,[36,37] while we differentiated DCs in the presence of CH223191 to test if AHR inhibition induced per se a pro-inflammatory skew. DC-10s were used as tolerogenic reference (Figure 4A).

AHR activation did not affect DC yield, while AHR inhibition significantly reduced it (Figure S4A). Despite efficient modulation of the AHR pathway, as indicated by upregulation and downregulation of CYP1B1 gene expression in ITE-treated DCs (AHRactDCs) and CH223191-treated DCs (AHRinhDCs), respectively, compared with DCs, we observed very limited phenotypic differences when comparing AHR-modulated DCs with DCs (Figures 4B, S4B, and S4C). Expression of DC-10 markers was similar (CD16, CD141, CD163, CD83, HLA-G, ILT-4) or significantly downregulated (CD14 and CD141), and DC markers (DC-SIGN, CD206, CD1a, and CD86) were mostly comparable in AHRactDCs compared with DCs. Most of the tested markers were unaffected in AHRinhDCs, while the fraction of CD1a+ and CD86+ cells was significantly lower and higher, respectively, compared with DCs (Figures 4B, S4C, and S4D).

We then tested the ability of AHR-modulated DCs to induce allogeneic T cell proliferation in a short-term MLR (Figure 4A). As expected, DC-10-primed T cells showed significantly lower proliferation, activation, and IFNγ production, compared with DC-primed T cells. Conversely, AHRactDC-primed T cells showed proliferation and activation profiles similar to that of DC-primed T cells, with a significantly higher IFNγ production (Figure 4C). Accordingly, IL-10 expression was not increased, while IL-6 expression was significantly upregulated in AHRactDCs vs. DCs (Figure S4E). These data indicate that AHR activation, in these DC differentiation conditions, is not sufficient per se to induce DCs with tolerogenic phenotype and function. AHRinhDCs showed reduced CD1a expression (see Figures 4B, S4C, and S4D), suggesting impaired DC differentiation. To test both stimulating ability of the bulk population and priming ability of fully differentiated DCs, we used both total and naive CD4+ T cells as responders in short-term MLR. Proliferation, activation, and IFNγ production of AHRinhDC-stimulated total CD4+ T cells were mildly, although significantly,
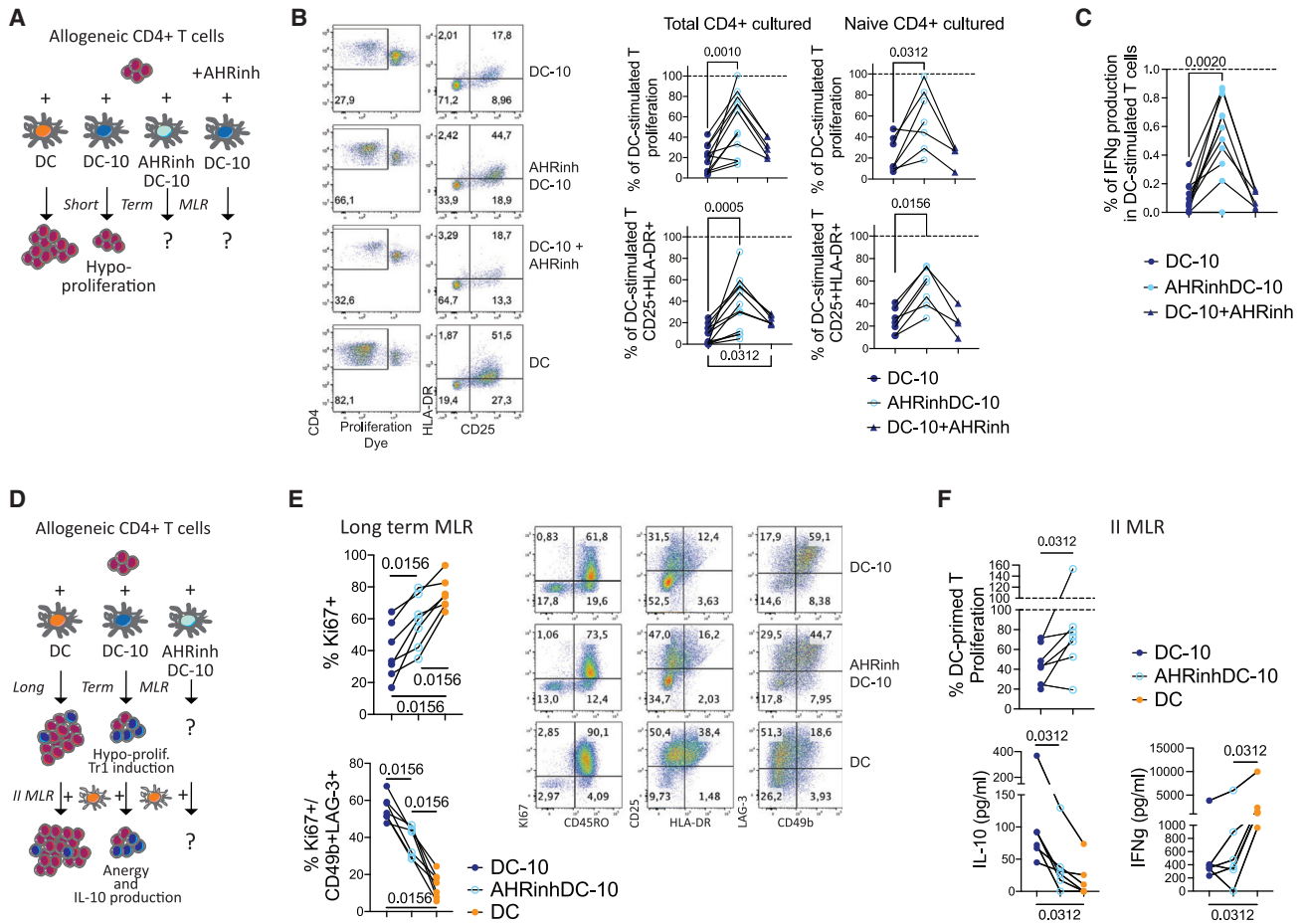
Figure 3. AHR activation is necessary for IL-10-induced tolerogenic functions in tolDCs generated *in vitro*

(A) Short-term MLR experimental design. DC stimulation of allogeneic CD4$^+$ T cells for 5 days induces T cell proliferation, while DC-10 stimulation induces T cell hypo-proliferation.

(B) Left, representative plots of proliferation dye dilution (left plots) and CD25 and HLA-DR expression (right plots). Right, percentages of proliferating (top) and CD25$^+$HLA-DR$^+$ activated (bottom) cells after co-culture of total (left graphs, n = 12) and naive (right graphs, n = 7) CD4$^+$ T cells with DC-10s, AHRinhDC-10s, and DC-10s in the presence of AHR inhibitor, relative to the results obtained with donor-matched DC-stimulated T, set at 100% (dotted line).

(C) IFNγ production by CD4$^+$ T cells (total and naive) stimulated with DC-10s, AHRinhDC-10s, and DC-10s in presence of AHR inhibitor, expressed as ratios to the IFNγ production of T cells stimulated by donor-matched DCs, set at 1 (dotted line) (n = 11).

(D) Long-term and secondary (II) MLR experimental design. DC stimulation of allogeneic CD4$^+$ T cells for 10 days induces T cell proliferation, DC-10 stimulation induces T cell hypo-proliferation and generation of Tr1 cells. II MLR: upon re-stimulation with mature DCs from the same donor used in priming, DC-primed T cells proliferate, while DC-10-primed T cells are anergic and produce IL-10.

(E) Long-term MLR. Left, percentage of CD4$^+$ cells proliferating (Ki67$^+$; top) and of Tr1 cells (CD49b$^+$LAG3$^+$; bottom) upon stimulation with DC-10s, AHRinhDC-10s, and DCs (n = 7). Right, representative FC plots.

(F) II MLR. Top, percentage of proliferation of T cells primed with the indicated DCs and restimulated with mature DCs from the same donor used in priming, expressed as (% proliferating cells/% proliferating cells in the donor-matched T cells primed with DCs) (n = 7); 0% = no proliferation; 100% = proliferated as DC-stimulated. Bottom, IL-10 and IFNγ amounts in culture supernatants (n = 6). p values by Wilcoxon matched pairs test. See Figure S3.

increased compared with that of DC-stimulated T cells, confirming the pleiotropic functions of AHR in addition to its roles in IL-10-mediated mechanisms (Figure 4D, top panels, and Figure S4F). Conversely, AHRinhDC-primed naive CD4$^+$ T cells showed increased activation and IFNγ production and decreased proliferation compared with DC-primed T cells (Figure 4D, bottom panels, and Figure S4F). These data confirmed that, in our differentiation conditions, AHR is needed for the differentiation of functional DCs and helps restraining a pro-inflammatory phenotype in monocytes.

IL-10 can inhibit the activity of mechanistic target of Rapamycin kinase (MTOR), which in turn can activate HIF1a, an antagonist of AHR activity.[12,38–40] IL-10 suppression of MTOR activity is mediated by the upregulation of the MTOR inhibitor DDIT4 (also known as REDD1/RTP801).[38,41] We found that DC-10s expressed significantly higher levels of DDIT4 compared with DCs (Figure 4E), suggesting that IL-10 may induce AHR-mediated tolerogenic features by inhibiting the MTOR pathway. To assess this hypothesis, we tested AHR activation, phenotype, and tolerogenic functions of DC-10s differentiated in presence of different concentrations of
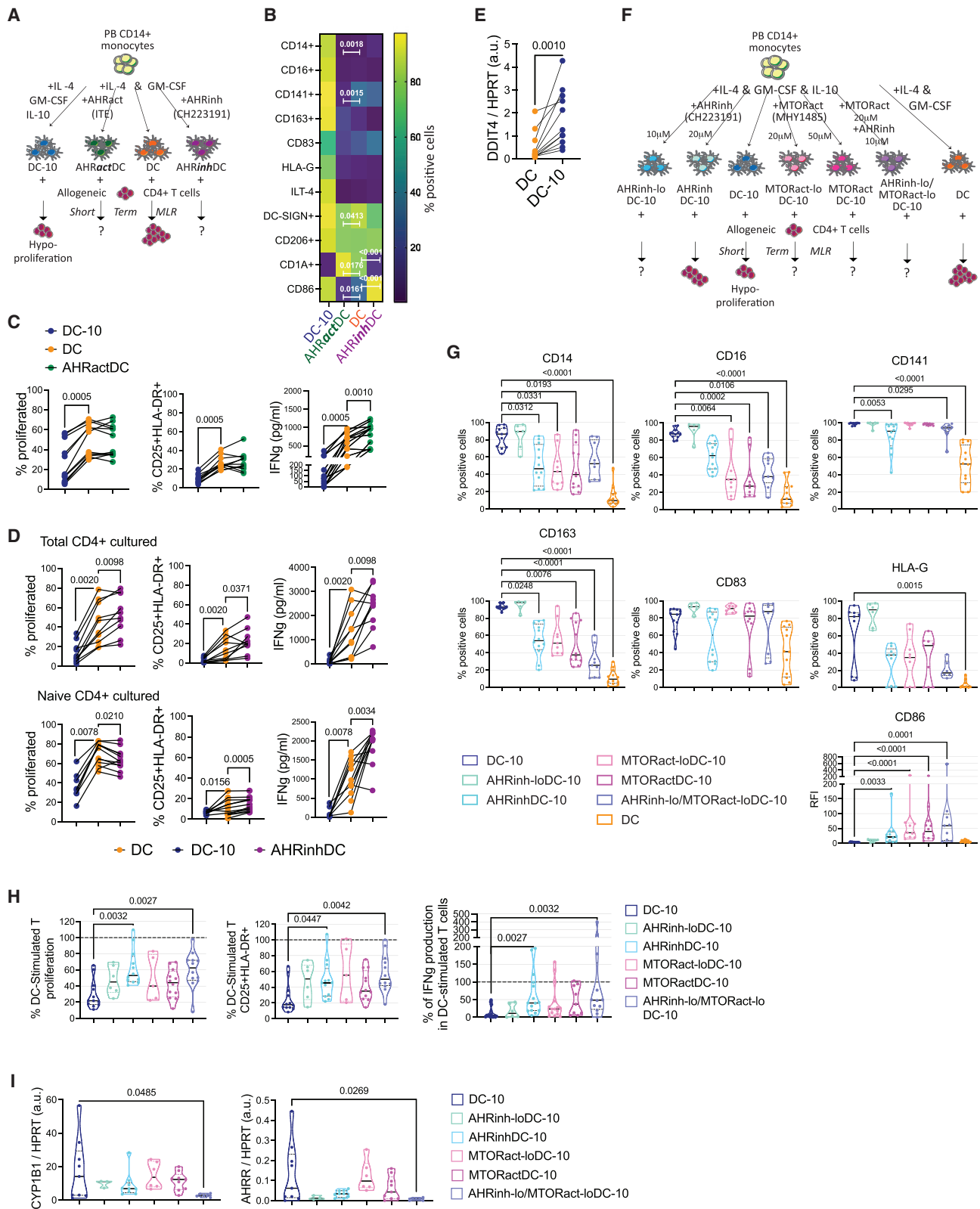
(legend on next page)

the MTOR activator MHY1485 (20 and 50 μM, MTORact-loDC-10s and MTORactDC-10s, respectively), as compared with DC-10s differentiated in the presence of different doses of CH223191 (10 and 20 μM, AHRinh-loDC-10s and AHRinhDC-10s, respectively) and untreated DC-10s. We also tested the effect of the two drugs combined (10 μM CH223191 + 20 μM MHY1485, AHRinh-lo/MTORact-loDC-10s) (Figure 4F). We confirmed efficient MHY1485-induced MTOR activation by assessing phosphorylation of MTOR target ribosomal protein S6 in DC-10s, MTORact-loDC-10s, and MTORactDC-10s (Figure S4G). If MTOR inhibition is needed for IL-10-mediated AHR activation, we would expect MTOR-activated DC-10s to lose tolerogenic features and AHR activation, similar to what is observed in AHRinhDC-10s. Moreover, the combination of the two drugs should show an additive effect, since used at the suboptimal doses (combination of the highest doses was toxic, data not shown). AHRinh-loDC-10s expressed DC-10 markers and CD86 at levels similar to DC-10s, while DC-10 marker loss and upregulation of CD86 was confirmed in AHRinhDC-10s. MTORactDC-10s and MTORact-loDC-10s showed a significant dose-dependent loss of DC-10 markers and upregulation of CD86, which were in the range of the changes observed in AHRinhDC-10s (Figure 4G). AHRinh-lo/MTORact-loDC-10s showed significantly decreased percentages of cells expressing CD16, CD141, and CD163 and increased expression of CD86 compared with DC-10s, to an extent that was compatible with an additive effect between the two drugs. In a short-term MLR, significant increases in proliferation, activation, and IFNγ production for AHRinhDC-10-stimulated T cells, as compared with DC-10-stimulated T cells, were confirmed (Figures 4H and S4H). Compared with DC-10-stimulated T cells, AHRinh-loDC-10-, MTORact-loDC-10-, and MTORactDC-10-stimulated T cells showed a trend toward higher proliferation, activation and IFNγ production that did not reach significance. Like AHRinhDC-10-stimulated cells, AHRinh-lo/MTORact-loDC-10-stimulated T cells displayed significantly higher proliferation, activation, and IFNγ production compared with DC-10s. Consistently, we found a tendency for a dose-dependent decrease in CYP1B1 and AHRR expression in AHR-inhibited and MTOR-activated DC-10s, while only AHRinh-lo/MTORact-loDC-10s reached significantly lower levels of AHR targets as compared with DC-10s (Figure 4I).

These data indicate that MTOR activity impacts negatively on the differentiation of DC-10s by antagonizing AHR activity and suggest that IL-10 may induce AHR activation by inhibiting the MTOR pathway.

AHR exploits IL-10-induced enhancers to establish tolerogenic signature in DCs

We then investigated the molecular mechanisms underlying loss of tolerogenic activities in AHRinhDC-10s. DC-10s produce high levels of IL-6 and IL-10, the latter mediating their regulatory activity.[17] We found, consistent with MLR results, that AHRinhDC-10s expressed significantly lower levels of IL-10 and IL-6 genes compared with DC-10s (Figure 5A).

To assess how AHR inhibition affects IL-10-induced genomic signature in tolDC, we performed ATAC-seq and RNA-seq on AHRinhDC-10s and compared results with those obtained in DC-10s. Even if AHR inhibition severely impacted overall chromatin accessibility, with 5,505 peaks lost in AHRinhDC-10s vs. DC-10s (Figure 5B), DC-10-specific enhancer accessibility was barely reduced (p = 0.008), considering the large sample size, in AHRinhDC-10s compared with DC-10s. This indicates that DC-10-specific enhancer accessibility is not dependent on AHR activity. Interestingly, AHR-dependent peaks overlapped with annotated promoters to a significantly higher extent than DC-10-specific peaks, suggesting that AHR inhibition had major effects on promoter activity and transcription (Figure S5A). Consistently, transcriptome was profoundly altered in AHRinhDC-10s, with

Figure 4. AHR-induced tolerogenic features are dependent on IL-10 and MTOR pathway inhibition

(A–D) Peripheral blood (PB) CD14+ monocytes were differentiated for 7 days in the presence of GM-CSF, IL-4 and IL-10 (DC-10), GM-CSF, and IL-4 without (DC) or with the AHR agonist ITE (30 μM) (AHRactDC) or the AHR inhibitor CH223191 (20 μM) (AHRinhDC).

(A) Experimental design.

(B) Heatmap displaying the median percentage of positive cells expressing the indicated marker in DC-10s, AHRactDCs, DCs, and AHRactDCs at 7 days of differentiation (n = 11–25). p values by Mixed effect model with Geisser-Greenhouse correction followed by Sidak's multiple comparison test; only AHRinhDC vs. DC and AHRactDC vs. DC p values are shown, the complete list of significant p values is shown in Figure S4C.

(C) Short-term MLR of total CD4+ T cells stimulated with DC-10s, DCs, and AHRactDCs (n = 12). Percentages of proliferating (left) and CD25+HLA-DR+ activated (middle) CD4+ cells, and IFNγ production (right) in the culture supernatants of. p values by Wilcoxon matched pairs test.

(D) Short-term MLR of total (top panels) and naive (bottom panels) CD4+ T cells stimulated with DC-10s, DCs, and AHRinhDCs (n = 10). Percentages of proliferating (left) and of CD25+HLA-DR+ activated (middle) CD4+ cells; IFNγ production (right) in the culture supernatants. p values by Wilcoxon matched pairs test.

(E) DDIT4 expression by ddPCR in DCs and DC-10s expressed as ratio of DDIT4 molecules/mL to HPRT molecules/mL in arbitrary units (a.u.). p value by Wilcoxon matched pairs test (n = 11).

(F) Experimental design describing DC differentiation conditions and short-term MLR assay. Peripheral blood (PB) CD14+ monocytes were differentiated for 7 days in the presence of GM-CSF and IL-4 (DC), GM-CSF, IL-4, and IL-10 (DC-10) without or with AHR antagonist CH223191 (10 μM, AHRinh-loDC-10; 20 μM, AHRinhDC-10), MTOR activator MHY1485 (20 μM, MTORact-loDC-10; 50 μM, MTORactDC-10), or the combination of CH223191 (10 μM) and MHY1485 (20 μM) (AHRinh-lo/MTORact-loDC-10).

(G) Percentages of positive cells or relative fluorescence intensity (RFI) for the indicated markers in the indicated conditions gated on CD11c+ Live/Dead negative population (n = 6–12).

(H) Percentages of proliferating (left) and CD25+HLA-DR+ activated (middle) cells, and IFNγ production in the supernatant (right) of total CD4+ T cells stimulated with DC-10s, AHRinh-lo DC-10s, AHRinhDC-10s, MTORact-lo DC-10s, MTORactDC-10s, or AHRinh-lo/MTORact-lo DC-10s, relative to the results obtained with donor-matched DC-stimulated T, set at 100% (dotted line) (n = 6–15).

(I) Expression of AHR targets CYP1B1 (left) and AHRR (right) by ddPCR. Arbitrary units (a.u.) are expressed as ratio between molecules/μL of the target gene and molecules/μL of the reference HPRT gene. (G–I) Median, interquartile range and single values are displayed. (F–H) p values by Kruskal-Wallis test followed by Dunn's multiple comparison test. See Figure S4.
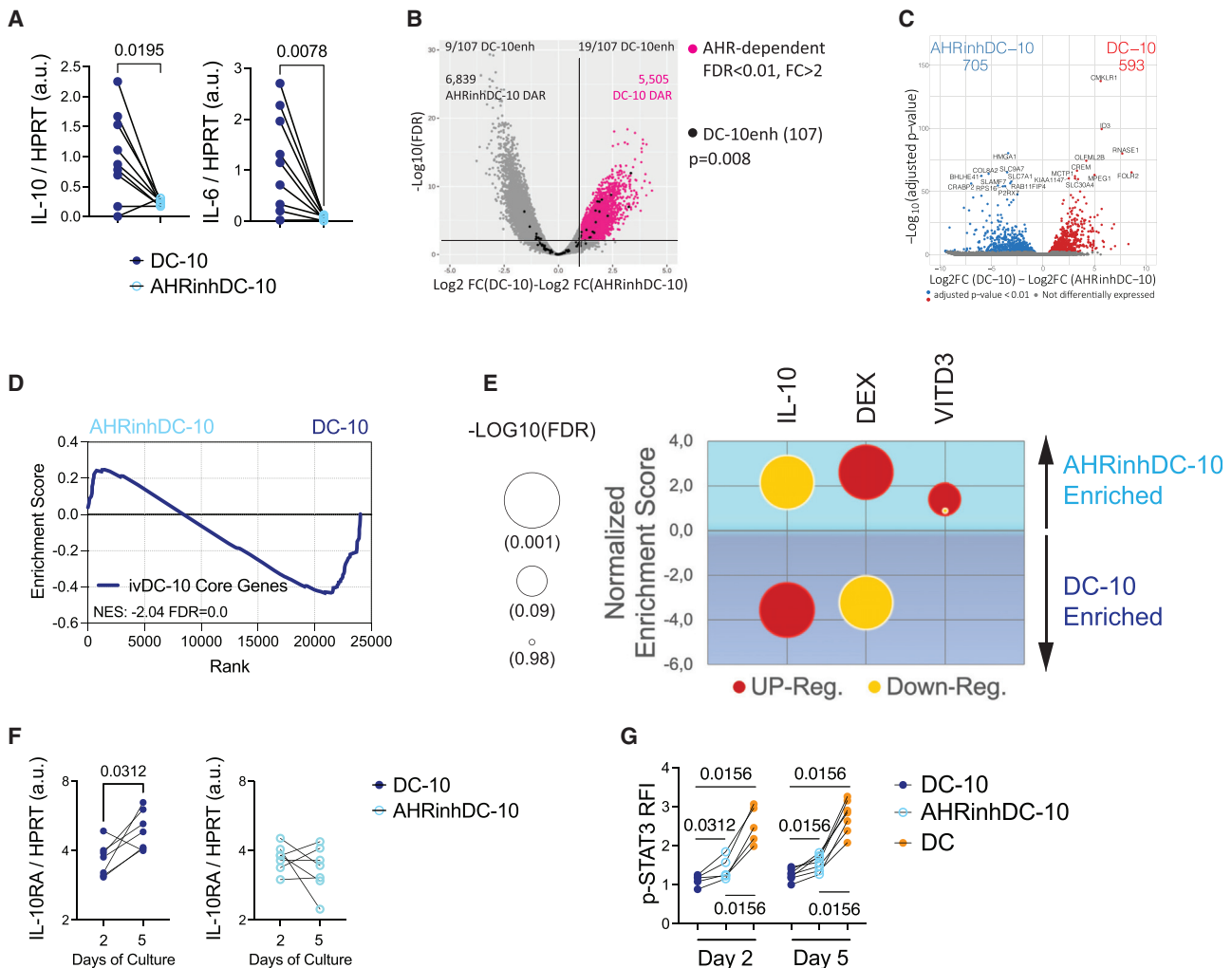
Figure 5. AHR activity controls IL-10-induced gene expression patterns

(A) Ratio of the indicated transcripts in molecules/μL to HPRT molecules/μL in arbitrary units (a.u.) by ddPCR in DC-10s and AHRinhDC-10s.

(B and C) Volcano plots of differentially accessible regions (DARs) by ATAC-seq (B) and differentially expressed genes (DEGs) by RNA-seq (C) in DC-10s and AHRinhDC-10s.

(B) Horizontal line at p = 0.01. Vertical line at logFC = 1. Gray dots = peaks obtained from the DC-10 vs. AHRinhDC-10 analysis; black dots = 107 DC-10-specific enhancers obtained in the DC-10 vs. DC analysis (see Figure 1D), the number of DC-10-specific enhancers enriched in DC-10 and AHRinhDC-10 peaks (p < 0.05) is indicated; pink dots = peaks accessible in DC-10s and not in AHRinhDC-10s. p value by Fisher's exact test. The number of DARs in the two conditions is indicated.

(C) Gray dots = non-differential genes; Red dots = DEGs (p < 0.01). Ten most significant DEGs in each group are indicated.

(D) GSEA of the 91 DC-10 core genes in the AHRinhDC-10 vs. DC-10 transcriptomes. Normalized enrichment score (NES) and FDR q-value are indicated.

(E) NES (y axis) and FDR q-value (dot size, expressed as -Log10) by GSEA of gene sets upregulated (red bubbles) and downregulated (yellow bubbles) in monocytes upon 24 h of IL-10 exposure (IL-10; GSE59184), in dexamethasone-induced (DEX) tolDC[42] and in Vitamin D3-induced tolDC (VITD3; GSE13762), assessed in AHRinhDC-10 vs. DC-10 transcriptomes. Blue area = DC-10 enriched, light blue area = AHRinhDC-10 enriched.

(F) IL-10 receptor alpha (IL10RA) expression by ddPCR in DC-10s and AHRinhDC-10s at 2 and 5 days of *in vitro* differentiation expressed as the ratio of IL-10 molecules/μL to HPRT molecules/μL in arbitrary units (a.u.).

(G) Phosphorylated-STAT3 (p-STAT3) fluorescence intensity (RFI) by flow cytometry (FC) of IL-10-stimulated, relative to -unstimulated, DC-10s, AHRinhDC-10s, and DCs at days 2 and 5 of differentiation. (A, F, and G) p values by Wilcoxon matched pairs test. See Figure S5.

705 and 593 genes downregulated and upregulated, respectively, compared with DC-10s (Figure 5C). As expected, genes downregulated in AHRinhDC-10s were strongly enriched in gene targets of TFs controlled by AHR, such as MAF and NFE2L2 (Figures S5B and S5C).

The expression of DC-10 core genes was significantly depleted in AHRinhDC-10 transcriptome, confirming that AHR activity is required for the expression of DC-10 core genes (Figure 5D). Notably, genes upregulated in AHRinhDC-10s were enriched in classes linked to

inflammation (Figure S5D), leading us to investigate whether AHR activity is more broadly involved in promoting tolerogenic pathways in DCs. We found genes upregulated in monocytes upon IL-10 exposure (Table S3)[42–45] significantly depleted in AHRinhDC-10s, confirming that IL-10-induced gene expression relies on AHR activity (Figure 5E). On the contrary, genes upregulated in dexamethasone (DEX)- and Vitamin D3 (VITD3)-induced tolDC (Table S3)[42–45] were enriched in AHRinhDC-10 transcriptome. Of note, genes downregulated in DEX tolDCs were enriched in DC-10 transcriptome (Figure 5E). The inverse correlation between AHR inhibition and gene expression patterns associated with IL-10, but not with those associated with other types of tolDCs, supports a specific link between AHR activity and IL-10-induced pathways.

The documented transcriptional control of IL-10RA by AHR in intestinal epithelial cells[46] and the effect of AHR inhibition on genes controlled by IL-10 led us to verify whether AHR inhibition prevented the ability of monocytes to sense IL-10. We assessed IL-10RA expression in AHRinhDC-10s and DC-10s at day 2 of differentiation and observed comparable levels. At day 5, DC-10s upregulated IL-10RA expression, while AHRinhDC-10s did not (Figure 5F). We tested STAT3 phosphorylation in response to IL-10 stimulation and found a significantly higher phosphorylation in AHRinhDC-10s compared with DC-10s at days 2 and 5 of differentiation (Figures 5G and S5E), indicating efficient IL-10R signaling in AHRinhDC-10s. DC-10s showed the lowest STAT3 phosphorylation compared with DCs and AHRinhDC-10s, very likely because of negative feedback mechanisms activated by the exposure to IL-10 during differentiation. These data ruled out a direct effect of AHR inhibition on IL-10 sensing during tolDC differentiation.

The IL-10/AHR genomic signature is active *in vivo* and is altered in autoimmune conditions

To determine whether the IL-10/AHR genomic signature identified in *in vitro* differentiated DC-10s is relevant in *ex vivo* isolated DC-10s (evDC-10s),[17,18] we analyzed chromatin accessibility in evDC-10s and their inflammatory counterpart classical DCs (cDCs) (Figure S6A). Chromatin accessibility was markedly different between the two cell types, with around 10,000 peaks specifically accessible in evDC-10s and not in cDCs (Figure 6A). When testing the distribution of the 107 DC-10-specific enhancers identified *in vitro* (Figure 1D), we found them significantly enriched among evDC-10 peaks vs. cDC peaks ($p = 3 \times 10^{-7}$; Figure 6A), suggesting that most of the enhancers used by *in vitro* DC-10s are also used by DC-10s *in vivo*. Moreover, the 91 DC-10 core genes (Table S1 and Figure 1D) were highly significantly enriched in the transcriptome of evDC-10s vs. cDCs (Figure S6B), supporting a common chromatin signature between *in vitro* and *ex vivo* DC-10s.

FANTOM5 database[21] intersection identified 1,105 robust enhancers among the evDC-10-specific peaks and 643 putative enhancer target genes (Table S4). Using TFmotifView,[47] we investigated whether the most enriched TF binding sites in *in vitro* differentiated DC-10s (Figure 1F, light blue and peach clouds) were also enriched in evDC-10 enhancer and target gene promoter sequences. While BACH2 and NFE2 binding sites

were not enriched in *in vitro* or *ex vivo* sequences by this analysis (not shown), all the other TF binding sites enriched in *in vitro* DC-10 sequences were significantly enriched also in evDC-10s (Figure 6B). MAF and AHR/ARNT binding sites were enriched in enhancers and promoters, respectively, in *in vitro* and *ex vivo* DC-10s, indicating that these TFs are relevant for DC-10 biology. Moreover, BATF binding sites were enriched in both enhancers and promoters *in vitro* and *ex vivo*, suggesting a key role for BATF, already described in Tregs upstream of AHR activation,[25] in this context. Interestingly, in AHRinhDC-10s we observed enrichment of AHR/ARNT and MAF binding sites in both enhancers and promoters, while BATF binding sites were enriched in promoters only. In AHRinhDC-10s, BATF binding sites were maintained in enhancers, thus we postulated that BATF binding to the enhancer is independent, and likely upstream, of the AHR network. Accordingly, we found that BATF transcription was activated very early upon IL-10 stimulation of monocytes (Figure S6C).

We then assessed the presence of an AHR pan-tissue signature recently described[14] in evDC-10 transcriptome. AHR signature was significantly enriched in both *in vitro* and *ex vivo* DC-10s, and, as expected, significantly depleted in *in vitro* AHRinhDC-10s (Figure 6C), further supporting a role for the AHR in *in vivo* DC-10s.

We finally investigated the relevance of our results for human physiology and studied DC-10s in a severe autoimmune condition, relapsing remitting multiple sclerosis (MS). We differentiated *in vitro* DC-10s from peripheral blood (PB) monocytes of MS patients and healthy controls (HCs). We observed significantly lower percentages of CD163+ cells in MS DC-10s compared with HCs (Figure S6D), suggesting impaired differentiation of MS DC-10s. Accordingly, MS DC-10-primed T cells had a significantly higher proliferation and activation rate compared with HC DC-10-primed T cells (Figure 6D). These data indicate that *in vitro* differentiated MS DC-10s are functionally defective. To test if these defects were linked to alterations in AHR-related pathways in differentiated DC-10s or their monocyte progenitors, we performed RNA-seq on MS and HC *in vitro* differentiated and *ex vivo* isolated DC-10s, and reanalyzed published RNA-seq data obtained from relapsing remitting MS and HC monocytes.[48] Unsupervised analysis revealed negligible differences in the transcriptomes of MS and HC DC-10s, both *in vitro* and *ex vivo* (Figure S6E). Nevertheless, the expression of the 91 DC-10 core genes, AHR pan-tissue signature genes,[14] and genes upregulated in peripheral blood mononuclear cells (PBMCs) upon IL-10 stimulation (MSigDB: GSE43700; Table S3)[49] were significantly depleted in *in vitro* differentiated MS DC-10s compared with HC DC-10s, correlating with the functional defects observed in MS DC-10s (Figure 6E). Conversely, the three gene lists were significantly enriched in the transcriptome of *ex vivo* isolated MS monocytes, as compared with HC monocytes. Significant enrichment of DC-10 core genes was also observed in *ex vivo* DC-10s isolated from MS patients as compared with HCs, while the enrichment in IL-10-induced genes was lost in these cells (Figure 6E).

Since tryptophan metabolism, the main source of AHR ligands, and chronic activation of interleukin signaling have been associated with cellular senescence,[50–53] we tested
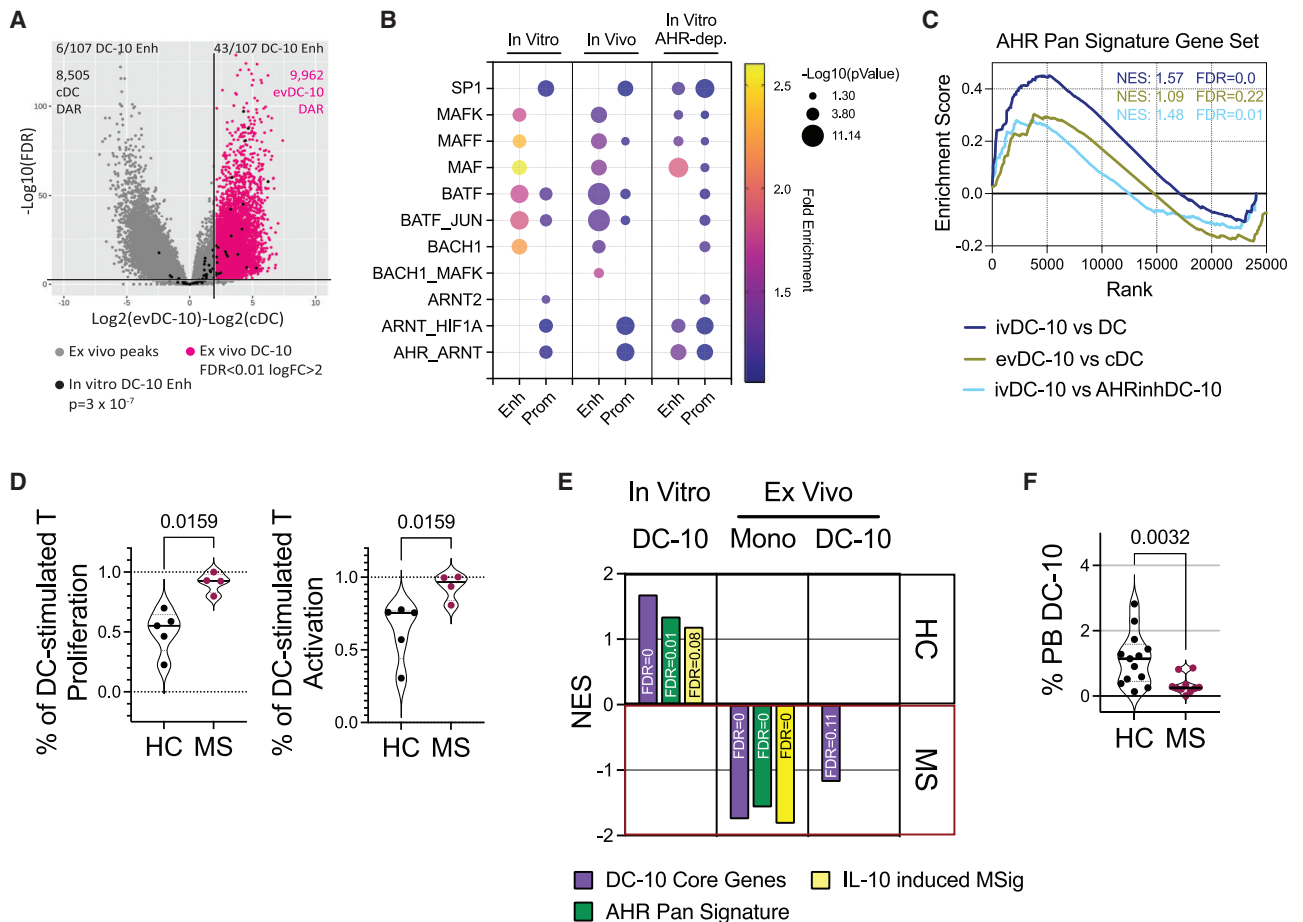
Figure 6. IL-10/AHR signature is active *in vivo* and is altered in autoimmune conditions

(A) DESeq2 volcano plot of ATAC peaks in evDC-10s (n = 6) and cDCs (n = 4) plotting log2(FC) and -log10 (FDR). Horizontal line at p = 0.01. Vertical line at logFC = 2. Gray dots = peaks obtained from the evDC-10 vs. cDC analysis; black dots = 107 DC-10-specific enhancers obtained in *in vitro* DC-10 vs. DC analysis (see Figure 1D), the number of DC-10-specific enhancers enriched in cDC and evDC-10 peaks (p < 0.05) are indicated, together with the number of differentially accessible regions (DARs); pink dots = accessible peaks in evDC-10s and not in cDCs. p value by Fisher's exact test.

(B) Bubble plot of indicated TF binding site enrichment by TFmotifView: p value (bubble size) and fold enrichment (bubble color) over background in robust enhancer (enh) and target gene promoter (prom) sequences specific for DC-10s (*in vitro*) and evDC-10s (*in vivo*) and lost in AHRinhDC-10s (*in vitro* AHR dep.). p values >0.05 are not displayed.

(C) GSEA of AHR pan signature gene set in ivDC-10s vs. DCs (blue, leading-edge genes: 70 of 166), evDC-10s vs. cDCs (green, leading-edge genes; 40 of 166) and ivDC-10s vs. AHRinhDC-10s (light blue, leading-edge genes: 31 of 166) transcriptomes. Normalized enrichment score (NES) and FDR are reported.

(D) HC and MS monocytes were differentiated into DCs and DC-10s tested in short-term MLR. Left, percentage of DC-stimulated T cell proliferation expressed as % proliferating DC-10-primed CD4⁺/% donor-matched proliferating DC-primed CD4⁺; right, percentage of DC-stimulated T activation expressed as %CD25⁺ and/or HLA-DR⁺ DC-10-primed CD4⁺/% donor-matched CD25⁺ and/or HLA-DR⁺ DC-primed CD4⁺. HC: T cells stimulated by healthy monocyte-derived DC-10s; MS: T cells stimulated by multiple sclerosis-derived DC-10s. Violin plots display median, interquartile range, and single values.

(E) Normalized enrichment score (NES) by GSEA of the 91 DC-10 core (purple), AHR pan signature[14] (green), and IL-10-induced molecular signature (MSigDB: GSE43700) (yellow) genes in the transcriptomes of healthy (HC) vs. multiple sclerosis (MS) *in vitro* differentiated DC-10s (left), monocytes (middle), and *ex vivo* isolated DC-10s (right). FDR is provided for each gene set. Only significantly enriched gene sets are shown. Details on gene lists used are provided in Tables S2 and S3. Number of leading genes in each group are provided in Table S6.

(F) Violin plot displaying median, interquartile range, and single values of the percentage of DC-10s (CD14⁺CD16⁺CD141⁺CD163⁺) in the PB of healthy controls (HC) and multiple sclerosis (MS) donors. (D and F) p value by Mann-Whitney test, n = 4–5 (D), n = 10–13 (F). See Figure S6.

whether MS monocytes, which displayed upregulated IL-10-induced AHR-mediated pathways, showed signs of senescence in their transcriptome, which may result in reduced fitness and inability to respond efficiently to IL-10 and differentiate into DC-10s *in vitro*. Eight out of the 11 senescence-associated molecular signatures tested were significantly enriched in MS

compared with HC monocytes by GSEA (Table S3; Figure S6F). Accordingly, the percentage of circulating DC-10s in the PB was significantly lower in MS patients as compared with HCs, even if the expression of DC-10 markers/tolerogenic molecules was not significantly different (Figures 6F and S6G). Overall, these data indicate that IL-10-induced AHR-mediated pathways are altered

in MS DC-10s and DC-10 precursors and that these alterations correlate with inefficient DC-10 differentiation both *in vitro* and *in vivo*.

DISCUSSION

We investigated the molecular mechanisms induced by IL-10 during the differentiation of human tolDCs and identified that AHR activation is required for the establishment of IL-10-induced core genes and tolerogenic functions in human DCs. We report here a role for AHR downstream of IL-10 signaling in myeloid cells. Indeed, AHR-specific inhibition in DC-10s leads to loss of expression of IL-10-induced core genes, IL-10 itself, and key tolerogenic molecules (ILT-4, HLA-G, and PD-L1). The *in vitro* IL-10/AHR genomic signature is also present in DC-10s *in vivo*, suggesting a role for the identified pathways in tolDC *in vivo* differentiation. Underlying the relevance of the described signature for human health, DC-10s derived from MS patients' monocytes showed significant downregulation of the expression of identified IL-10/AHR-activated core genes, correlating with severe defects in tolerogenic functions.

The combined assessment of chromatin status and transcriptome in IL-10-induced tolDCs allowed us to identify a restricted list of core genes that seems to be necessary for the function of IL-10 in these conditions. Among them, ILT-4 and IRF-1 may play key roles. Indeed, we and others have shown IL-10-dependent upregulation of ILT-4 expression mediating tolerogenic functions in monocyte-derived DCs.[17,54] IRF-1 can directly control IL-10 gene expression, but its activity seems to be related to the cellular context, as it can induce both tolerogenic (in T and cancer cells) and pro-inflammatory (in T and myeloid cells) gene expression patterns.[25,55–59] A full understanding of the role of the identified core genes requires further investigation and might allow the discovery of additional IL-10 functions.

We showed that AHR-specific inhibition in DC-10s resulted in loss of their tolerogenic functions, providing evidence for the necessity of AHR activity in IL-10-mediated induction of tolerance in myeloid cells. AHR is a ligand-induced TF deeply studied as a critical modulator of immune cell functions and immune tolerance. Because of its promiscuity both in ligand and co-factor binding, its activity is strictly dependent on the cellular context in which it acts.[8–10] Most AHR studies have been performed in mice, where AHR can play both pro-inflammatory and tolerogenic functions in T cells, while it seems to induce tolerogenic mechanisms in DCs. In humans, AHR activation via tryptophan-derived metabolites has been shown to modulate monocyte-derived DCs.[34,35] However, activating AHR during DC differentiation in absence of IL-10 did not result in acquisition of tolerogenic activities, indicating that AHR activation is not sufficient per se to induce full tolDC differentiation in our differentiation conditions, and confirming that AHR activity is strongly context dependent. This is further supported by the results obtained in AHRinhDCs, which confirmed that AHR is needed for full DC differentiation[14] and restrains pro-inflammatory pathways in the monocyte/DC axis. Overall, modulation, both positive and negative, of AHR in DCs not exposed to IL-10 resulted in limited modulation of tolerogenic/pro-inflammatory phenotypes and functions as compared with results obtained by AHR modulation

in DC-10s. This further supports the evidence that AHR, beyond its previously described roles in modulating immune cells, specifically acts in DCs in an IL-10-dependent manner. Several studies have demonstrated that the IL-10 gene is a primary target of AHR transcriptional activity in various immune cells, including mouse DCs.[7,11,60,61] We demonstrate here that AHR functions downstream of IL-10 signaling. AHR gene transcription can be activated by STAT3, which mediates signaling of several cytokines, including IL-10, in mouse T cells.[12] Nevertheless, we found that AHR transcription is significantly lower in DC-10s compared with DCs and is downregulated at early time points upon IL-10 stimulation of monocytes, suggesting that IL-10-mediated induction of AHR activity does not occur at the transcriptional level.

IL-10 is a pleiotropic cytokine exerting opposite functions depending on the target cell and the molecular mechanisms involved. Nevertheless, its key role in controlling unwanted immune responses has been clearly demonstrated.[2,3] IL-10 signaling is mediated by phosphorylated STAT3, which directly activates gene transcription. STAT3 is known to cooperate with AHR to control specific cytokine gene loci in mouse T cells.[62,63] Along with the canonical immune pathways activated downstream of IL-10, recent studies have demonstrated that IL-10 also impacts cell metabolism. Indeed, IL-10 can inhibit MTOR activity while increasing mitophagy and oxidative phosphorylation (OXPHOS) in myeloid cells.[38,64,65] IL-10-induced catabolic pathways may induce the production of AHR ligands, while MTOR inhibition may block HIF1a, an inhibitor of AHR, thereby promoting AHR activity.[7,10,12,66] Both OXPHOS and MTOR pathways may play a role in IL-10-induced tolDCs. Nevertheless, our experiments showed that AHR-mediated tolerogenic features in IL-10-induced tolDCs are abrogated by MTOR activation, thus putting forth this pathway as a major player in AHR activation mediated by IL-10 in this system. OXPHOS has been associated with tolerogenic phenotypes in DCs.[64] Accordingly, OXPHOS-related genes can be induced by several factors currently used to generate tolDCs *in vitro*, such as VITD3 and DEX.[67,68] However, our data show that gene sets specifically upregulated in VITD3- and DEX-induced tolDCs are not enriched in the IL-10-induced transcriptome in DC-10s and are not dependent on AHR activity. These data indicate that, even converging on some specific key tolerogenic genes, different stimuli induce different tolerogenic pathways in monocyte-derived DCs, as previously proposed.[69]

Although AHR inhibition severely affected chromatin accessibility in DC-10s, likely by altering promoter activity, DC-10-specific enhancer accessibility was not lost in AHR-inhibited DC-10s, indicating that AHR does not play a primary role in establishing IL-10 chromatin signature. This role may be played by BATF, described as a key regulator of chromatin accessibility and gene expression patterns in the differentiation of mouse and human Tregs downstream of IL-27 and IL-33 signaling or OXPHOS metabolism.[25,70–77] We found BATF binding sites significantly enriched in DC-10 enhancers and maintained upon AHR inhibition, suggesting that BATF acts upstream of AHR. BATF expression was also upregulated at early timepoints in IL-10-stimulated monocytes. Through BATF upregulation, IL-10 may thus impact chromatin accessibility and allow activated AHR to bind

key regulatory elements. A similar mechanism has been described in IL-27-induced murine Tr1 cell differentiation, where BATF activity is required to establish genomic accessible regions, gene expression patterns, and AHR binding to the IL-10 gene.[25]

The IL-10-induced AHR signature characterized not only *in vitro* differentiated, but also *in vivo* occurring DC-10s, suggesting a physiological role for this molecular pattern in maintaining immune tolerance. Accordingly, the IL-10/AHR signature was significantly altered in monocytes and DC-10s isolated from MS patients, and this alteration correlated with defects in function and frequencies of *in vitro* and *in vivo* DC-10s, respectively.

MS is an autoimmune disease characterized by a CD4$^+$ T cell-triggered immune response against myelin antigens leading to severe neurodegeneration.[78] A correlation between MS disease and altered AHR pathways has been proposed by studies in the mouse model and in patients' plasma.[79–81] We provide here evidence of defects in the tolerogenic monocyte-DC axis in MS patients. Consistent with the defects in IL-10 pathways and Tr1 cell activity observed in MS patients,[82–84] our data show impaired ability of MS monocytes to respond to IL-10 and differentiate into functional tolDCs. Further studies are warranted to assess the molecular mechanisms (impaired expression of inhibitory molecules, secretion of cytokines or shedding of soluble CD163) underlying the observed defects and whether the observed alterations play a pathogenic role in MS development.

By identifying a molecular pattern induced by IL-10 in myeloid cells, our studies expand knowledge about the mechanisms controlling human tolerogenic immune cells. This knowledge, on one hand, improves our understanding of the molecular mechanisms controlling the maintenance of immune tolerance and, on the other hand, may help in designing therapies to re-establish it. Indeed, AHR has been already proposed as target of tolerogenic therapies, with beneficial effects already demonstrated in the mouse models of several autoimmune diseases. Upon discovery of the AHR activating and activated pathway downstream of IL-10, these could be manipulated *in vivo* to overcome possible defects of tolDCs in specific pathologies, and *in vitro* to enhance the differentiation of tolDCs for cell therapies.

Limitations of the study

We show that IL-10 imprints chromatin and transcriptome of differentiating DCs and that its tolerogenic activity is mainly mediated by AHR activation. Our study does not describe all the pathways/players activated by IL-10 and playing roles in establishing tolerogenic features in DCs. Moreover, it does not provide information on the specific molecular players acting upstream to establish the accessibility of IL-10-induced enhancers exploited by AHR, nor acting downstream of AHR and leading to the tolerogenic fate. Only further analysis of provided sequencing data and targeted experiments using our cellular model will address these issues.

By using an MTOR activator, we provide evidence for the need of MTOR inhibition to obtain IL-10/AHR-mediated tolDC differentiation and propose a direct effect of MTOR in inhibiting AHR by controlling HIF1a. Still, we cannot formally rule out an indirect contribution of autophagy to the system, as MTOR activation inevitably leads to inhibition of autophagy. Also, we have not as-

sessed the possible contribution of endogenous AHR ligands to the AHR activating pathways established downstream of IL-10.

By using AHR agonist ITE we provide evidence that, in our differentiating conditions, AHR activation is not sufficient per se to drive tolDC differentiation. This apparent contrast with published studies describing the ability of AHR to modulate DCs is likely explained by the strong DC differentiating conditions we used in our model. Nevertheless, we cannot exclude that the use of different AHR agonists, even in our differentiating conditions, will be more pro-tolerogenic than ITE, given the well-described context-specific activity of AHR agonists.

Finally, we describe a defect in the monocyte-DC axis in MS patients and link this defect to altered IL-10/AHR pathways. At this stage, we cannot assess whether the observed defects are causes or consequences of immune deregulation in these patients because the functional studies on DC-10 differentiation were performed on monocytes isolated from patients with active disease.

STAR★METHODS

Detailed methods are provided in the online version of this paper and include the following:

- KEY RESOURCES TABLE
- RESOURCE AVAILABILITY
  - ○ Lead contact
  - ○ Materials availability
  - ○ Data and code availability
- EXPERIMENTAL MODEL AND SUBJECT DETAILS
  - ○ Human subjects
  - ○ Cell preparation and DC differentiation
- METHOD DETAILS
  - ○ AHR and MTOR modulation
  - ○ Mixed lymphocyte reaction (MLR) assay
  - ○ Flow cytometry (FC) analysis
  - ○ Cytokine production by ELISA
  - ○ Cell sorting
  - ○ Gene expression analysis by droplet digital PCR (ddPCR)
  - ○ RNA-seq and microarray
  - ○ ATAC-seq
  - ○ ChIP-seq
  - ○ Enhancer identification and annotation
  - ○ Transcription factor motif identification
  - ○ Transcription factor network
  - ○ Feature alignment
  - ○ Gene set enrichment analysis (GSEA)
- QUANTIFICATION AND STATISTICAL ANALYSIS

AUTHOR CONTRIBUTIONS

D.A., investigation, software, formal analysis; A.T., software, formal analysis, data curation, validation; L.F., G.A., and M.V., investigation; V.M., resources; F.R.S.d.S., conceptualization, validation, formal analysis, investigation, writing – original draft, supervision; S.G., conceptualization, writing – original draft, supervision, funding acquisition.

DECLARATION OF INTERESTS

The authors declare no competing interests.

REFERENCES

1. Iberg, C.A., and Hawiger, D. (2020). Natural and induced tolerogenic dendritic cells. J. Immunol. *204*, 733–744. https://doi.org/10.4049/jimmunol.1901121.

2. Ouyang, W., and O'Garra, A. (2019). IL-10 family cytokines IL-10 and IL-22: from basic science to clinical translation. Immunity *50*, 871–891. https://doi.org/10.1016/j.immuni.2019.03.020.

3. Engelhardt, K.R., and Grimbacher, B. (2014). IL-10 in humans: lessons from the gut, IL-10/IL-10 receptor deficiencies, and IL-10 polymorphisms. Curr. Top. Microbiol. Immunol. *380*, 1–18. https://doi.org/10.1007/978-3-662-43492-5_1.

4. Lobo-Silva, D., Carriche, G.M., Castro, A.G., Roque, S., and Saraiva, M. (2016). Balancing the immune response in the brain: IL-10 and its regulation. J. Neuroinflammation *13*, 297–310. https://doi.org/10.1186/s12974-016-0763-8.

5. Saraiva, M., Vieira, P., and O'Garra, A. (2020). Biology and therapeutic potential of interleukin-10. J. Exp. Med. *217*, e20190418–e20190419. https://doi.org/10.1084/jem_20190418.

6. Gabryšová, L., Howes, A., Saraiva, M., and O'Garra, A. (2014). The regulation of IL-10 expression. Curr. Top. Microbiol. Immunol. *380*, 157–190. https://doi.org/10.1007/978-3-662-43492-5_8.

7. Apetoh, L., Quintana, F.J., Pot, C., Joller, N., Xiao, S., Kumar, D., Burns, E.J., Sherr, D.H., Weiner, H.L., and Kuchroo, V.K. (2010). The aryl hydrocarbon receptor interacts with c-Maf to promote the differentiation of type 1 regulatory T cells induced by IL-27. Nat. Immunol. *11*, 854–861. https://doi.org/10.1038/ni.1912.

8. Rothhammer, V., and Quintana, F.J. (2019). The aryl hydrocarbon receptor: an environmental sensor integrating immune responses in health and disease. Nat. Rev. Immunol. *19*, 184–197. https://doi.org/10.1038/s41577-019-0125-8.

9. Stockinger, B., Di Meglio, P., Gialitakis, M., and Duarte, J.H. (2014). The aryl hydrocarbon receptor: multitasking in the immune system. Annu. Rev. Immunol. *32*, 403–432. https://doi.org/10.1146/annurev-immunol-032713-120245.

10. Gutiérrez-Vázquez, C., and Quintana, F.J. (2018). Regulation of the immune response by the aryl hydrocarbon receptor. Immunity *48*, 19–33. https://doi.org/10.1016/j.immuni.2017.12.012.

11. Piper, C.J.M., Rosser, E.C., Oleinika, K., Nistala, K., Krausgruber, T., Rendeiro, A.F., Banos, A., Drozdov, I., Villa, M., Thomson, S., et al. (2019). Aryl hydrocarbon receptor contributes to the transcriptional program of IL-10-producing regulatory B cells. Cell Rep. *29*, 1878–1892.e7. https://doi.org/10.1016/j.celrep.2019.10.018.

12. Mascanfroni, I.D., Takenaka, M.C., Yeste, A., Patel, B., Wu, Y., Kenison, J.E., Siddiqui, S., Basso, A.S., Otterbein, L.E., Pardoll, D.M., et al. (2015). Metabolic control of type 1 regulatory T cell differentiation by AHR and HIF1-α. Nat. Med. *21*, 638–646. https://doi.org/10.1038/nm.3868.

13. Wei, P., Hu, G.H., Kang, H.Y., Yao, H.B., Kou, W., Liu, H., Zhang, C., and Hong, S.L. (2014). An aryl hydrocarbon receptor ligand acts on dendritic cells and T cells to suppress the Th17 response in allergic rhinitis patients. Lab. Invest. *94*, 528–535. https://doi.org/10.1038/labinvest.2014.8.

14. Sadik, A., Somarribas Patterson, L.F., Öztürk, S., Mohapatra, S.R., Panitz, V., Secker, P.F., Pfänder, P., Loth, S., Salem, H., Prentzell, M.T., et al. (2020). IL4I1 is a metabolic immune checkpoint that activates the AHR and promotes tumor progression. Cell *182*, 1252–1270.e34. https://doi.org/10.1016/j.cell.2020.07.038.

15. Baba, N., Rubio, M., Kenins, L., Regairaz, C., Woisetschlager, M., Carballido, J.M., and Sarfati, M. (2012). The aryl hydrocarbon receptor (AhR) ligand VAF347 selectively acts on monocytes and naïve CD4(+) Th cells to promote the development of IL-22-secreting Th cells. Hum. Immunol. *73*, 795–800. https://doi.org/10.1016/j.humimm.2012.05.002.

16. Goudot, C., Coillard, A., Villani, A.-C., Gueguen, P., Cros, A., Sarkizova, S., Tang-Huau, T.L., Bohec, M., Baulande, S., Hacohen, N., et al. (2017). Aryl hydrocarbon receptor controls monocyte differentiation into dendritic cells versus macrophages. Immunity *47*, 582–596.e6. https://doi.org/10.1016/j.immuni.2017.08.016.

17. Gregori, S., Tomasoni, D., Pacciani, V., Scirpoli, M., Battaglia, M., Magnani, C.F., Hauben, E., and Roncarolo, M.G. (2010). Differentiation of type 1 T regulatory cells (Tr1) by tolerogenic DC-10 requires the IL-10-dependent ILT4/HLA-G pathway. Blood *116*, 935–944. https://doi.org/10.1182/blood-2009-07-234872.

18. Comi, M., Avancini, D., Santoni de Sio, F., Villa, M., Uyeda, M.J., Floris, M., Tomasoni, D., Bulfone, A., Roncarolo, M.G., and Gregori, S. (2020). Coexpression of CD163 and CD141 identifies human circulating IL-10-producing dendritic cells (DC-10). Cell. Mol. Immunol. *17*, 95–107. https://doi.org/10.1038/s41423-019-0218-0.

19. Locafaro, G., Amodio, G., Tomasoni, D., Tresoldi, C., Ciceri, F., and Gregori, S. (2014). HLA-G expression on blasts and tolerogenic cells in patients affected by acute myeloid leukemia. J. Immunol. Res. *2014*, 636292. https://doi.org/10.1155/2014/636292.

20. Amodio, G., Mugione, A., Sanchez, A.M., Viganò, P., Candiani, M., Somigliana, E., Roncarolo, M.G., Panina-Bordignon, P., and Gregori, S. (2013). HLA-G expressing DC-10 and CD4+ T cells accumulate in human decidua during pregnancy. Hum. Immunol. *74*, 406–411. https://doi.org/10.1016/j.humimm.2012.11.031.

21. Andersson, R., Gebhard, C., Miguel-Escalada, I., Hoof, I., Bornholdt, J., Boyd, M., Chen, Y., Zhao, X., Schmidl, C., Suzuki, T., et al. (2014). An atlas of active enhancers across human cell types and tissues. Nature *507*, 455–461. https://doi.org/10.1038/nature12787.

22. Calo, E., and Wysocka, J. (2013). Modification of enhancer chromatin: what, how, and why? Mol. Cell *49*, 825–837. https://doi.org/10.1016/j.molcel.2013.01.038.

23. Li, W., Notani, D., and Rosenfeld, M.G. (2016). Enhancers as non-coding RNA transcription units: recent insights and future perspectives. Nat. Rev. Genet. *17*, 207–223. https://doi.org/10.1038/nrg.2016.4.

24. Roychoudhuri, R., Hirahara, K., Mousavi, K., Clever, D., Klebanoff, C.A., Bonelli, M., Sciumè, G., Zare, H., Vahedi, G., Dema, B., et al. (2013). BACH2 represses effector programs to stabilize T reg-mediated immune homeostasis. Nature *498*, 506–510. https://doi.org/10.1038/nature12199.

25. Karwacz, K., Miraldi, E.R., Pokrovskii, M., Madi, A., Yosef, N., Wortman, I., Chen, X., Watters, A., Carriero, N., Awasthi, A., et al. (2017). Critical role of IRF1 and BATF in forming chromatin landscape during type 1 regulatory

cell differentiation. Nat. Immunol. *18*, 412–421. https://doi.org/10.1038/ni.3683.

26. Szklarczyk, D., Gable, A.L., Lyon, D., Junge, A., Wyder, S., Huerta-Cepas, J., Simonovic, M., Doncheva, N.T., Morris, J.H., Bork, P., et al. (2019). STRING v11: protein-protein association networks with increased coverage, supporting functional discovery in genome-wide experimental datasets. Nucleic Acids Res. *47*, D607–D613. https://doi.org/10.1093/nar/gky1131.

27. Gandhi, R., Kumar, D., Burns, E.J., Nadeau, M., Dake, B., Laroni, A., Kozoriz, D., Weiner, H.L., and Quintana, F.J. (2010). Activation of the aryl hydrocarbon receptor induces human type 1 regulatory T cell-like and Foxp3+ regulatory T cells. Nat. Immunol. *11*, 846–853. https://doi.org/10.1038/ni.1915.

28. Quintana, F.J., Basso, A.S., Iglesias, A.H., Korn, T., Farez, M.F., Bettelli, E., Caccamo, M., Oukka, M., and Weiner, H.L. (2008). Control of Treg and TH17 cell differentiation by the aryl hydrocarbon receptor. Nature *453*, 65–71. https://doi.org/10.1038/nature06880.

29. Hauben, E., Gregori, S., Draghici, E., Migliavacca, B., Olivieri, S., Woisetschläger, M., and Roncarolo, M.G. (2008). Activation of the aryl hydrocarbon receptor promotes allograft-specific tolerance through direct and dendritic cell-mediated effects on regulatory T cells. Blood *112*, 1214–1222. https://doi.org/10.1182/blood-2007-08-109843.

30. Chng, S.H., Kundu, P., Dominguez-Brauer, C., Teo, W.L., Kawajiri, K., Fujii-Kuriyama, Y., Mak, T.W., and Pettersson, S. (2016). Ablating the aryl hydrocarbon receptor (AhR) in CD11c+ cells perturbs intestinal epithelium development and intestinal immunity. Sci. Rep. *6*, 23820. https://doi.org/10.1038/srep23820.

31. Zhao, B., DeGroot, D.E., Hayashi, A., He, G., and Denison, M.S. (2010). Ch223191 is a ligand-selective antagonist of the Ah (dioxin) receptor. Toxicol. Sci. *117*, 393–403. https://doi.org/10.1093/toxsci/kfq217.

32. Choi, E.-Y., Lee, H., Dingle, R.W.C., Kim, K.B., and Swanson, H.I. (2012). Development of novel CH223191-based antagonists of the aryl hydrocarbon receptor. Mol. Pharmacol. *81*, 3–11. https://doi.org/10.1124/mol.111.073643.

33. Gagliani, N., Magnani, C.F., Huber, S., Gianolini, M.E., Pala, M., Licona-Limon, P., Guo, B., Herbert, D.R., Bulfone, A., Trentini, F., et al. (2013). Co-expression of CD49b and LAG-3 identifies human and mouse T regulatory type 1 cells. Nat. Med. *19*, 739–746. https://doi.org/10.1038/nm.3179.

34. Wang, C., Ye, Z., Kijlstra, A., Zhou, Y., and Yang, P. (2014). Activation of the aryl hydrocarbon receptor affects activation and function of human monocyte-derived dendritic cells. Clin. Exp. Immunol. *177*, 521–530. https://doi.org/10.1111/cei.12352.

35. Jurado-Manzano, B.B., Zavala-Reyes, D., Turrubiartes-Martínez, E.A., Portales-Pérez, D.P., González-Amaro, R., and Layseca-Espinosa, E. (2017). FICZ generates human tDCs that induce CD4+ CD25high Foxp3+ Treg-like cell differentiation. Immunol. Lett. *190*, 84–92. https://doi.org/10.1016/j.imlet.2017.07.013.

36. Song, J., Clagett-Dame, M., Peterson, R.E., Hahn, M.E., Westler, W.M., Sicinski, R.R., and DeLuca, H.F. (2002). A ligand for the aryl hydrocarbon receptor isolated from lung. Proc. Natl. Acad. Sci. USA *99*, 14694–14699. https://doi.org/10.1073/pnas.232562899.

37. Goettel, J.A., Gandhi, R., Kenison, J.E., Yeste, A., Murugaiyan, G., Sambanthamoorthy, S., Griffith, A.E., Patel, B., Shouval, D.S., Weiner, H.L., et al. (2016). AHR activation is protective against colitis driven by T cells in humanized mice. Cell Rep. *17*, 1318–1329. https://doi.org/10.1016/j.celrep.2016.09.082.

38. Ip, W.K.E., Hoshi, N., Shouval, D.S., Snapper, S., and Medzhitov, R. (2017). Anti-inflammatory effect of IL-10 mediated by metabolic reprogramming of macrophages. Science *356*, 513–519. https://doi.org/10.1126/science.aal3535.

39. Hudson, C.C., Liu, M., Chiang, G.G., Otterness, D.M., Loomis, D.C., Kaper, F., Giaccia, A.J., and Abraham, R.T. (2002). Regulation of hypoxia-inducible factor 1α expression and function by the mammalian target

of rapamycin. Mol. Cell Biol. *22*, 7004–7014. https://doi.org/10.1128/mcb.22.20.7004-7014.2002.

40. Majumder, P.K., Febbo, P.G., Bikoff, R., Berger, R., Xue, Q., McMahon, L.M., Manola, J., Brugarolas, J., McDonnell, T.J., Golub, T.R., et al. (2004). mTOR inhibition reverses Akt-dependent prostate intraepithelial neoplasia through regulation of apoptotic and HIF-1-dependent pathways. Nat. Med. *10*, 594–601. https://doi.org/10.1038/nm1052.

41. Brugarolas, J., Lei, K., Hurley, R.L., Manning, B.D., Reiling, J.H., Hafen, E., Witters, L.A., Ellisen, L.W., and Kaelin, W.G. (2004). Regulation of mTOR function in response to hypoxia by REDD1 and the TSC1/TSC2 tumor suppressor complex. Genes Dev. *18*, 2893–2904. https://doi.org/10.1101/gad.1256804.

42. García-González, P.A., Schinnerling, K., Sepúlveda-Gutiérrez, A., Maggi, J., Mehdi, A.M., Nel, H.J., Pesce, B., Larrondo, M.L., Aravena, O., Molina, M.C., et al. (2017). Dexamethasone and monophosphoryl lipid a induce a distinctive profile on monocyte- derived dendritic cells through transcriptional modulation of genes associated with essential processes of the immune response. Front. Immunol. *8*, 1350. https://doi.org/10.3389/fimmu.2017.01350.

43. Montoya, D., Inkeles, M.S., Liu, P.T., Realegeno, S., Teles, R.M.B., Vaidya, P., Munoz, M.A., Schenk, M., Swindell, W.R., Chun, R., et al. (2014). IL-32 is a molecular marker of a host defense network in human tuberculosis. Sci. Transl. Med. *6*, 250ra114. https://doi.org/10.1126/scitranslmed.3009546.

44. Széles, L., Keresztes, G., Töröcsik, D., Balajthy, Z., Krenács, L., Póliska, S., Steinmeyer, A., Zuegel, U., Pruenster, M., Rot, A., and Nagy, L. (2009). 1,25-dihydroxyvitamin D3 is an autonomous regulator of the transcriptional changes leading to a tolerogenic dendritic cell phenotype. J. Immunol. *182*, 2074–2083. https://doi.org/10.4049/jimmunol.0803345.

45. Popov, A., Driesen, J., Abdullah, Z., Wickenhauser, C., Beyer, M., Debey-Pascher, S., Saric, T., Kummer, S., Takikawa, O., Domann, E., et al. (2008). Infection of myeloid dendritic cells with Listeria monocytogenes leads to the suppression of T cell function by multiple inhibitory mechanisms. J. Immunol. *181*, 4976–4988. https://doi.org/10.4049/jimmunol.181.7.4976.

46. Lanis, J.M., Alexeev, E.E., Curtis, V.F., Kitzenberg, D.A., Kao, D.J., Battista, K.D., Gerich, M.E., Glover, L.E., Kominsky, D.J., and Colgan, S.P. (2017). Tryptophan metabolite activation of the aryl hydrocarbon receptor regulates IL-10 receptor expression on intestinal epithelia. Mucosal Immunol. *10*, 1133–1144. https://doi.org/10.1038/mi.2016.133.

47. Leporcq, C., Spill, Y., Balaramane, D., Toussaint, C., Weber, M., and Bardet, A.F. (2020). TFmotifView: a webserver for the visualization of transcription factor motifs in genomic regions. Nucleic Acids Res. *48*, W208–W217. https://doi.org/10.1093/nar/gkaa252.

48. Kim, K., Pröbstel, A.K., Baumann, R., Dyckow, J., Landefeld, J., Kogl, E., Madireddy, L., Loudermilk, R., Eggers, E.L., Singh, S., et al. (2021). Cell type-specific transcriptomics identifies neddylation as a novel therapeutic target in multiple sclerosis. Brain *144*, 450–461. https://doi.org/10.1093/brain/awaa421.

49. Teles, R.M.B., Graeber, T.G., Krutzik, S.R., Montoya, D., Schenk, M., Lee, D.J., Komisopoulou, E., Kelly-scumpia, K., Chun, R., Iyer, S.S., et al. (2013). Type I interferon suppresses type II interferon–triggered human anti-mycobacterial responses. Science *339*, 1448–1453.

50. Kondrikov, D., Elmansi, A., Bragg, R.T., Mobley, T., Barrett, T., Eisa, N., Kondrikova, G., Schoeinlein, P., Aguilar-Perez, A., Shi, X.M., et al. (2020). Kynurenine inhibits autophagy and promotes senescence in aged bone marrow mesenchymal stem cells through the aryl hydrocarbon receptor pathway. Exp. Gerontol. *130*, 110805. https://doi.org/10.1016/j.exger.2019.110805.

51. Castro-Portuguez, R., and Sutphin, G.L. (2020). Kynurenine pathway, NAD+ synthesis, and mitochondrial function: targeting tryptophan metabolism to promote longevity and healthspan. Exp. Gerontol. *132*, 110841. https://doi.org/10.1016/j.exger.2020.110841.

52. Rea, I.M., Gibson, D.S., McGilligan, V., McNerlan, S.E., Alexander, H.D., and Ross, O.A. (2018). Age and age-related diseases: role of inflammation triggers and cytokines. Front. Immunol. *9*, 586–628. https://doi.org/10.3389/fimmu.2018.00586.

53. Kuilman, T., Michaloglou, C., Vredeveld, L.C.W., Douma, S., van Doorn, R., Desmet, C.J., Aarden, L.A., Mooi, W.J., and Peeper, D.S. (2008). Oncogene-induced senescence relayed by an interleukin-dependent inflammatory network. Cell *133*, 1019–1031. https://doi.org/10.1016/j.cell.2008.03.039.

54. Saito, M., Nagasawa, M., Takada, H., Hara, T., Tsuchiya, S., Agematsu, K., Yamada, M., Kawamura, N., Ariga, T., Tsuge, I., et al. (2011). Defective IL-10 signaling in hyper-IgE syndrome results in impaired generation of tolerogenic dendritic cells and induced regulatory T cells. J. Exp. Med. *208*, 235–249. https://doi.org/10.1084/jem.20100799.

55. Ziegler-Heitbrock, L., Lötzerich, M., Schaefer, A., Werner, T., Frankenberger, M., and Benkhart, E. (2003). IFN-A induces the human IL-10 gene by recruiting both IFN regulatory factor 1 and Stat3. J. Immunol. *171*, 285–290. https://doi.org/10.4049/jimmunol.171.1.285.

56. Qiao, Y., Giannopoulou, E.G., Chan, C.H., Park, S.-H., Gong, S., Chen, J., Hu, X., Elemento, O., and Ivashkiv, L.B. (2013). Synergistic activation of inflammatory cytokine genes by interferon-γ-induced chromatin remodeling and toll-like receptor signaling. Immunity *39*, 454–469. https://doi.org/10.1016/j.immuni.2013.08.009.

57. Yan, Y., Zheng, L., Du, Q., Yan, B., and Geller, D.A. (2020). Interferon regulatory factor 1 (IRF-1) and IRF-2 regulate PD-L1 expression in hepatocellular carcinoma (HCC) cells. Cancer Immunol. Immunother. *69*, 1891–1903. https://doi.org/10.1007/s00262-020-02586-9.

58. Chistiakov, D.A., Myasoedova, V.A., Revin, V.V., Orekhov, A.N., and Bobryshev, Y.V. (2018). The impact of interferon-regulatory factors to macrophage differentiation and polarization into M1 and M2. Immunobiology *223*, 101–111. https://doi.org/10.1016/j.imbio.2017.10.005.

59. Kano, S.i., Sato, K., Morishita, Y., Vollstedt, S., Kim, S., Bishop, K., Honda, K., Kubo, M., and Taniguchi, T. (2008). The contribution of transcription factor IRF1 to the interferon-gamma-interleukin 12 signaling axis and TH1 versus TH-17 differentiation of CD4+ T cells. Nat. Immunol. *9*, 34–41. https://doi.org/10.1038/ni1538.

60. Nguyen, N.T., Kimura, A., Nakahama, T., Chinen, I., Masuda, K., Nohara, K., Fujii-Kuriyama, Y., and Kishimoto, T. (2010). Aryl hydrocarbon receptor negatively regulates dendritic cell immunogenicity via a kynurenine-dependent mechanism. Proc. Natl. Acad. Sci. USA *107*, 19961–19966. https://doi.org/10.1073/pnas.1014465107.

61. Kimura, A., Naka, T., Nakahama, T., Chinen, I., Masuda, K., Nohara, K., Fujii-Kuriyama, Y., and Kishimoto, T. (2009). Aryl hydrocarbon receptor in combination with Stat1 regulates LPS-induced inflammatory responses. J. Exp. Med. *206*, 2027–2035. https://doi.org/10.1084/jem.20090560.

62. Quintana, F.J., Jin, H., Burns, E.J., Nadeau, M., Yeste, A., Kumar, D., Rangachari, M., Zhu, C., Xiao, S., Seavitt, J., et al. (2012). Aiolos promotes TH17 differentiation by directly silencing Il2 expression. Nat. Immunol. *13*, 770–777. https://doi.org/10.1038/ni.2363.

63. Yeste, A., Mascanfroni, I.D., Nadeau, M., Burns, E.J., Tukpah, A.M., Santiago, A., Wu, C., Patel, B., Kumar, D., and Quintana, F.J. (2014). IL-21 induces IL-22 production in CD4+ T cells. Nat. Commun. *5*, 3753. https://doi.org/10.1038/ncomms4753.

64. O'Neill, L.A.J., and Pearce, E.J. (2016). Immunometabolism governs dendritic cell and macrophage function. J. Exp. Med. *213*, 15–23. https://doi.org/10.1084/jem.20151570.

65. Gopinathan, U., Øvstebø, R., Brusletto, B.S., Olstad, O.K., Kierulf, P., Brandtzaeg, P., and Berg, J.P. (2017). Transcriptomic data from two primary cell models stimulating human monocytes suggest inhibition of oxidative phosphorylation and mitochondrial function by N . meningitidis which is partially up- regulated by IL-10. BMC Immunol. *18*, 1–17. https://doi.org/10.1186/s12865-017-0229-5.

66. He, L., Gomes, A.P., Wang, X., Yoon, S.O., Lee, G., Nagiec, M.J., Cho, S., Chavez, A., Islam, T., Yu, Y., et al. (2018). mTORC1 promotes metabolic reprogramming by the suppression of GSK3-dependent Foxk1 phosphorylation. Mol. Cell *70*, 949–960.e4. https://doi.org/10.1016/j.molcel.2018.04.024.

67. Ferreira, G.B., Vanherwegen, A.S., Eelen, G., Gutiérrez, A.C.F., VanLommel, L., Marchal, K., Verlinden, L., Verstuyf, A., Nogueira, T., Georgiadou, M., et al. (2015). Vitamin D3 induces tolerance in human dendritic cells by activation of intracellular metabolic pathways. Cell Rep. *10*, 711–725. https://doi.org/10.1016/j.celrep.2015.01.013.

68. Rachamim, N., Latter, H., Malinin, N., Asher, C., Wald, H., and Garty, H. (1995). Dexamethasone enhances expression of mitochondrial oxidative phosphorylation genes in rat distal colon. Am. J. Physiol. *269*, C1305–C1310. https://doi.org/10.1152/ajpcell.1995.269.5.C1305.

69. Navarro-Barriuso, J., Mansilla, M.J., Naranjo-Gómez, M., Sánchez-Pla, A., Quirant-Sánchez, B., Teniente-Serra, A., Ramo-Tello, C., and Martínez-Cáceres, E.M. (2018). Comparative transcriptomic profile of tolerogenic dendritic cells differentiated with vitamin D3, dexamethasone and rapamycin. Sci. Rep. *8*, 14985–15013. https://doi.org/10.1038/s41598-018-33248-7.

70. Delacher, M., Imbusch, C.D., Hotz-Wagenblatt, A., Mallm, J.-P., Bauer, K., Simon, M., Riegel, D., Rendeiro, A.F., Bittner, S., Sanderink, L., et al. (2020). Precursors for nonlymphoid-tissue Treg cells reside in secondary lymphoid organs and are programmed by the transcription factor BATF. Immunity *52*, 295–312.e11. https://doi.org/10.1016/j.immuni.2019.12.002.

71. Delacher, M., Simon, M., Sanderink, L., Hotz-Wagenblatt, A., Wuttke, M., Schambeck, K., Schmidleithner, L., Bittner, S., Pant, A., Ritter, U., et al. (2021). Single-cell chromatin accessibility landscape identifies tissue repair program in human regulatory T cells. Immunity *54*, 702–720.e17. https://doi.org/10.1016/j.immuni.2021.03.007.

72. Koizumi, S.-I., Sasaki, D., Hsieh, T.-H., Taira, N., Arakaki, N., Yamasaki, S., Wang, K., Sarkar, S., Shirahata, H., Miyagi, M., and Ishikawa, H. (2018). JunB regulates homeostasis and suppressive functions of effector regulatory T cells. Nat. Commun. *9*, 5344. https://doi.org/10.1038/s41467-018-07735-4.

73. Delacher, M., Imbusch, C.D., Weichenhan, D., Breiling, A., Hotz-Wagenblatt, A., Träger, U., Hofer, A.C., Kägebein, D., Wang, Q., Frauhammer, F., et al. (2017). Genome-wide DNA-methylation landscape defines specialization of regulatory T cells in tissues. Nat. Immunol. *18*, 1160–1172. https://doi.org/10.1038/ni.3799.

74. Shin, B., Benavides, G.A., Geng, J., Koralov, S.B., Hu, H., Darley-Usmar, V.M., and Harrington, L.E. (2020). Mitochondrial oxidative phosphorylation regulates the fate decision between pathogenic Th17 and regulatory T cells. Cell Rep. *30*, 1898–1909.e4. https://doi.org/10.1016/j.celrep.2020.01.022.

75. Alvisi, G., Brummelman, J., Puccio, S., Mazza, E.M., Tomada, E.P., Losurdo, A., Zanon, V., Peano, C., Colombo, F.S., Scarpa, A., et al. (2020). IRF4 instructs effector Treg differentiation and immune suppression in human cancer. J. Clin. Invest. *130*, 3137–3150. https://doi.org/10.1172/JCI130426.

76. Vasanthakumar, A., Moro, K., Xin, A., Liao, Y., Gloury, R., Kawamoto, S., Fagarasan, S., Mielke, L.A., Afshar-Sterle, S., Masters, S.L., et al. (2015). The transcriptional regulators IRF4, BATF and IL-33 orchestrate development and maintenance of adipose tissue-resident regulatory T cells. Nat. Immunol. *16*, 276–285. https://doi.org/10.1038/ni.3085.

77. Hayatsu, N., Miyao, T., Tachibana, M., Murakami, R., Kimura, A., Kato, T., Kawakami, E., Endo, T.A., Setoguchi, R., Watarai, H., et al. (2017). Analyses of a mutant Foxp3 allele reveal BATF as a critical transcription factor in the differentiation and accumulation of tissue regulatory T cells. Immunity *47*, 268–283.e9. https://doi.org/10.1016/j.immuni.2017.07.008.

78. Dendrou, C.A., Fugger, L., and Friese, M.A. (2015). Immunopathology of multiple sclerosis. Nat. Rev. Immunol. *15*, 545–558. https://doi.org/10.1038/nri3871.

79. Quintana, F.J., Murugaiyan, G., Farez, M.F., Mitsdoerffer, M., Tukpah, A.-M., Burns, E.J., and Weiner, H.L. (2010). An endogenous aryl hydrocarbon

receptor ligand acts on dendritic cells and T cells to suppress experimental autoimmune encephalomyelitis. Proc. Natl. Acad. Sci. USA 107, 20768–20773. https://doi.org/10.1073/pnas.1009201107.

80. Tsaktanis, T., Beyer, T., Nirschl, L., Linnerbauer, M., Grummel, V., Bussas, M., Tjon, E., Mühlau, M., Korn, T., Hemmer, B., et al. (2021). Aryl hydrocarbon receptor plasma agonist activity correlates with disease activity in progressive MS. Neurol. Neuroimmunol. Neuroinflamm. 8, e933. https://doi.org/10.1212/NXI.0000000000000933.

81. Rothhammer, V., Borucki, D.M., Garcia Sanchez, M.I., Mazzola, M.A., Hemond, C.C., Regev, K., Paul, A., Kivisäkk, P., Bakshi, R., Izquierdo, G., et al. (2017). Dynamic regulation of serum aryl hydrocarbon receptor agonists in MS. Neurol. Neuroimmunol. Neuroinflamm. 4, e359. https://doi.org/10.1212/NXI.0000000000000359.

82. Martinez-Forero, I., Garcia-Munoz, R., Martinez-Pasamar, S., Inoges, S., Lopez-Diaz de Cerio, A., Palacios, R., Sepulcre, J., Moreno, B., Gonzalez, Z., Fernandez-Diez, B., et al. (2008). IL-10 suppressor activity and ex vivo Tr1 cell function are impaired in multiple sclerosis. Eur. J. Immunol. 38, 576–586. https://doi.org/10.1002/eji.200737271.

83. Hu, D., Notarbartolo, S., Croonenborghs, T., Patel, B., Cialic, R., Yang, T.H., Aschenbrenner, D., Andersson, K.M., Gattorno, M., Pham, M., et al. (2017). Transcriptional signature of human pro-inflammatory TH17 cells identifies reduced IL10 gene expression in multiple sclerosis. Nat. Commun. 8, 1600. https://doi.org/10.1038/S41467-017-01571-8.

84. Astier, A.L., Meiffren, G., Freeman, S., and Hafler, D.A. (2006). Alterations in CD46-mediated Tr1 regulatory T cells in patients with multiple sclerosis. J. Clin. Invest. 116, 3252–3257. https://doi.org/10.1172/JCI29251.

85. Chen, E.Y., Tan, C.M., Kou, Y., Duan, Q., Wang, Z., Meirelles, G.V., Clark, N.R., and Ma'ayan, A. (2013). Enrichr : interactive and collaborative HTML5 gene list enrichment analysis tool. BMC Bioinf. 14, 128.

86. Zhou, Y., Zhou, B., Pache, L., Chang, M., Khodabakhshi, A.H., Tanaseichuk, O., Benner, C., and Chanda, S.K. (2019). Metascape provides a biologist-oriented resource for the analysis of systems-level datasets. Nat. Commun. 10, 1523. https://doi.org/10.1038/s41467-019-09234-6.

87. Gopinathan, U., Ovstebø, R., Olstad, O.K., Brusletto, B., Dalsbotten Aass, H.C., Kierulf, P., Brandtzaeg, P., and Berg, J.P. (2012). Global effect of interleukin-10 on the transcriptional profile induced by Neisseria meningitidis in human monocytes. Infect. Immun. 80, 4046–4054. https://doi.org/10.1128/IAI.00386-12.

88. Corces, M.R., Trevino, A.E., Hamilton, E.G., Greenside, P.G., Sinnott-armstrong, N.A., Vesuna, S., Satpathy, A.T., Rubin, A.J., Montine, K.S., Wu, B., et al. (2017). An improved ATAC- seq protocol reduces background and enables interrogation of frozen tissues. Nat. Methods 14, 959–962. https://doi.org/10.1038/nmeth.4396.

89. Marzetta, F., Simó-Riudalbas, L., Duc, J., Planet, E., Verp, S., Turelli, P., and Trono, D. (2019). The KZFP/KAP1 system controls transposable elements-embedded regulatory sequences in adult T cells. Preprint at bioRxiv. https://doi.org/10.1101/523597.

90. Thomas-Chollier, M., Darbo, E., Herrmann, C., Defrance, M., Thieffry, D., and Van Helden, J. (2012). A complete workflow for the analysis of full-size ChIP-seq (and similar) data sets using peak-motifs. Nat. Protoc. 7, 1551–1568. https://doi.org/10.1038/nprot.2012.088.

91. Subramanian, A., Tamayo, P., Mootha, V.K., Mukherjee, S., Ebert, B.L., Gillette, M.A., Paulovich, A., Pomeroy, S.L., Golub, T.R., Lander, E.S., and Mesirov, J.P. (2005). Gene set enrichment analysis: a knowledge-based approach for interpreting genome-wide expression profiles. Proc. Natl. Acad. Sci. USA 102, 15545–15550. https://doi.org/10.1073/PNAS.0506580102.

STAR★METHODS

KEY RESOURCES TABLE

REAGENT or RESOURCE	SOURCE	IDENTIFIER
Antibodies		
Anti human CD1a-FITC	BD Pharmingen	Cat# 555806;RRID:AB_396140
Anti human CD1a-PE	BD Pharmingen	Cat# 555807;RRID:AB_396141
Anti human CD1c-FITC	Miltenyi Biotec	Cat# 130-104-894;RRID:AB_2661158
Anti human CD4-APC	BD Pharmingen	Cat# 345771; RRID:AB_2868799
Anti human CD4-PECy7	BD Pharmingen	Cat# 557852;RRID:AB_396897
Anti human CD11c-FITC	BD Pharmingen	Cat# 561355; RRID:AB_10611872
Anti human CD11c-PECy7	BD Pharmingen	Cat# 561356;RRID:AB_10611859
Anti human CD14-FITC	BD	Cat# 345784; RRID:AB_2868810
Anti human CD14-PerCPCy5.5	BioLegend	Cat# 325622; RRID:AB_893250
Anti human CD14-APC-H7	BD Pharmingen	Cat# 560180;RRID:AB_1645464
Anti human CD16-Alexa647	BD	Cat# 557710; RRID:AB_396819
Anti human CD16-PB	BD	Cat# 558122;RRID:AB_397042
Anti human CD16-BV510	BD	Cat# 563830
Anti human CD25-APC	BD Biosciences	Cat# 340907; RRID:AB_2819021
Anti human CD25-BV421	BD Biosciences	Cat# 562442; RRID:AB_11154578
Anti human CD25-PE	BD	Cat# 341011;RRID:AB_2783790
Anti human CD45RA-FITC	BD Biosciences	Cat# 555488; RRID:AB_395879
Anti human CD45RO-PerCPCy5.5	BioLegend	Cat# 304221; RRID:AB_1575041
Anti human CD49b-APC	Miltenyi Biotec	Cat# 130-100-396; RRID:AB_2658464
Anti human CD83-BV786	BD	Cat# 565336; RRID:AB_2739191
Anti human CD83-BUV737	BD Biosciences	Cat# 612823; RRID:AB_2870147
Anti human CD83-PECy7	BD	Cat# 561132; RRID:AB_10562565
Anti human CD86-PE-CF594	BD	Cat# 562390; RRID:AB_11154047
Anti human CD86-PerCPCy5.5	BD Biosciences	Cat# 561129; RRID:AB_10562395
Anti human CD141-BV421	BD	Cat# 565321; RRID:AB_2739180
Anti human CD141-BV711	BD Biosciences	Cat# 563155; RRID:AB_2738033
Anti human CD141-PE	Miltenyi Biotec	Cat# 130090514;RRID:AB_244173
Anti human CD163-PerCPCy5.5	BD	Cat# 563887; RRID:AB_2738467
Anti human CD163-BV421	BD Biosciences	Cat# 562643; RRID:AB_2737697
Anti human CLEC4G-APC	R&D Systems	Cat# FAB2947A
Anti human DC-SIGN (CD209)-PE	BD	Cat# 551265; RRID:AB_394123
Anti human HLA-G-APC	EXBIO	Cat# 1A-292-C100; RRID:AB_10734198
Anti human HLA-G-PE	EXBIO	Cat# 1P-437-C100; RRID:AB_10736118
Anti human HLA-DR-BV510	BD Biosciences	Cat# 563083; RRID:AB_2737994
Anti human HLA-DR-PE	BD Pharmingen	Cat# 555561; RRID:AB_395943
Anti human ILT-4-APC	R&D Systems	Cat# FAB2078A; RRID:AB_663839
Anti human LAG3-PE	Miltenyi Biotec	Cat# 130-120-470;RRID:AB_2784078
Anti human PDL1-PE	eBioscience	Cat# 12-5983-42
Anti human Phospho-S6 (Ser235, Ser236)-PECy7	Thermo Scientific	Cat# 25-9007-42
Anti human phosphoSTAT3 (PY705)-Alexa647	BD Phosflow	Cat# 557815;RRID:AB_647144
Purified Rat Anti-Human and Viral IL-10 (clone JES3-9D7)	BD Biosciences	Cat# 554497:RRID:AB_395433
Purified Mouse Anti-Human IFNg (clone NIB42)	BD Biosciences	Cat# 551221;RRID:AB_394099

Continued

REAGENT or RESOURCE	SOURCE	IDENTIFIER
Biotin Anti-Human and Viral IL-10 (clone JES3-12G8)	BD Biosciences	Cat# 554499; RRID:AB_395435
Biotin Anti-Human IFNg (clone 4S.B3)	BD Biosciences	Cat# 554550; RRID:AB_395472
Recombinant Human IL-10 protein	Cell Genix	Cat# 1414-050
Recombinant Human IFNg	R&D Systems	Cat# 285-IF100
Anti H3K27ac	Abcam	Cat# ab4729; RRID:AB_2118291
Anti H3K4me1	Abcam	Cat# ab8895; RRID:AB_306847
Anti H3K9me3	Abcam	Cat# ab8898 ;RRID:AB_306848
Chemicals, peptides, and recombinant proteins		
CH-223191	Invivogen	Cat# INH-CH22
ITE	Invivogen	Cat# tlrl-ite
MHY1485	Calbiochem	Cat# 5005540001
Critical commercial assays		
Human CD14 MicroBeads	Miltenyi Biotec	Cat# 130-050-201
Human CD4 isolation kit	Miltenyi Biotec	Cat# 130-091-155
Human CD45RO MicroBeads	Miltenyi Biotec	Cat# 130-046-001
RNeasy Micro kit	Qiagen	Cat# 74034
miRNeasy Micro kit	Qiagen	Cat# 217084
Tagment DNA enzyme and buffer Small kit	Illumina	Cat# 20034197
Deposited data		
Ex vivo DC-10 and cDC RNA-seq	https://doi.org/10.1038/s41423-019-0218-0	GEO: GSE117945
IL-10 stimulated monocyte Microarray	https://doi.org/10.1186/s12865-017-0229-5	GEO: GSE82316
MS and HC monocyte RNA-seq	https://doi.org/10.1093/brain/awaa421	GEO: GSE137143
ATAC-seq *ex vivo* DC-10/DC	This paper	GEO: GSE180753
ATAC-seq *in vitro* DC-10/DC/AHRinhDC-10	This paper	GEO: GSE180754
RNA-seq *in vitro* DC-10/DC/AHRinhDC-10	This paper	GEO: GSE180761
RNA-seq *in vitro* DC-10 MS/HC	This paper	GEO: GSE180760
RNA-seq *ex vivo* DC-10 MS/HC	This paper	GEO: GSE180755
Oligonucleotides		
CYP1A1 FAM-Probe	Thermo-Fisher	Cat# Hs00153120
IL-6 FAM-Probe	Thermo-Fisher	Cat# Hs00985639
IL-10 FAM-Probe	Thermo-Fisher	Cat# Hs00174086
ILT-4 (LIRB2) EvaGreen	Bio-Rad	Cat# dHSaEG5020183
SOCS3 EvaGreen	Bio-Rad	Cat# dHSaEG5001979
HPRT VIC-probe	Bio-Rad	Cat# 1409017
Software and algorithms		
FlowJo v10	BD	https://www.flowjo.com/
Prism v9 and v10	GraphPad Software	https://www.graphpad.com/scientific-software/prism/
Morpheus	Broad Institute	https://software.broadinstitute.org/morpheus/
DESeq2	https://doi.org/10.1186/s13059-014-0550-8	https://bioconductor.org/packages/release/bioc/html/DESeq2.html
EnrichR	https://doi.org/10.1186/1471-2105-14-128	https://maayanlab.cloud/Enrichr/)
Metascape	https://doi.org/10.1186/1471-2105-14-128	metascape.org
DiffBind	http://bioconductor.org/packages/release/bioc/vignettes/DiffBind/inst/doc/DiffBind.pdf	https://bioconductor.org/packages/release/bioc/html/DiffBind.html
Regulatory Sequence Analysis Tools (RSAT)	https://doi.org/10.1038/nprot.2012.088	http://rsat.sb-roscoff.fr/
TFmotifView	https://doi.org/10.1093/nar/gkaa252	http://bardet.u-strasbg.fr/tfmotifview/

Continued

REAGENT or RESOURCE	SOURCE	IDENTIFIER
String	https://doi.org/10.1093/nar/gky1131	https://string-db.org
Gene Set Enrichment Analysis (GSEA)	https://doi.org/10.1073/PNAS.0506580102	https://www.gsea-msigdb.org/gsea/index.jsp
Other		
Recombinant human IL-4	Miltenyi Biotec	Cat# 130-093-922
Recombinant human GM-CSF	Miltenyi Biotec	Cat# 130-093-867
Recombinant human IL-10	Cell Genix	Cat# 1414-050

RESOURCE AVAILABILITY

Lead contact
Further information and requests for resources and reagents should be directed to and will be fulfilled by the lead contact, Silvia Gregori (gregori.silvia@hsr.it).

Materials availability
This study did not generate new unique reagents.

Data and code availability
- RNA-seq and ATAC-seq data have been deposited at GEO database and are publicly available as of the date of publication under the SuperSeries GSE180762. Accession numbers are listed in the key resources table. This paper analyzes existing, publicly available data. These accession numbers for the datasets are listed in the key resources table.
- This paper does not report original code.
- Any additional information required to reanalyze the data reported in this paper is available from the lead contact upon request.

EXPERIMENTAL MODEL AND SUBJECT DETAILS

Human subjects
Human peripheral blood was obtained from healthy donors on informed consent in accordance with the Declaration of Helsinki and under protocols approved by the ethical committee of the San Raffaele Telethon Institute for Gene Therapy (TIGET09, TIGET12B).

Relapsing remitting multiple sclerosis patients were enrolled in an active state of disease and in absence of treatment ($35,6 \pm 9.6$ years of age; 6M/6F). Healthy controls were matched to patients by sex and age ($33,5 \pm 8.7$ years of age; 4M/9F).

Cell preparation and DC differentiation
Peripheral blood mononuclear cells (PBMCs) were isolated from healthy peripheral blood by density gradient centrifugation over Lymphoprep (CEDARLANE) and washed with PBS. Red blood cells were lysed by incubation with ammonium chloride solution and platelets were removed by low-speed centrifugation.

CD14$^+$ monocytes were isolated from PBMCs by positive selection using CD14 MicroBeads (Miltenyi Biotec) according to manufacturer's instructions.

CD14$^+$ monocytes were differentiated into dendritic cells (DC) in RPMI 1640 medium (Lonza), 10% fetal bovine serum (FBS) (Euroclone), 100 U/mL penicillin/streptomycin (Lonza), and 2 mM L-glutamine (Lonza) at 10^6 cells/mL, in the presence of 100 ng/mL Recombinant Human GM-CSF (Miltenyi Biotec) and 10 ng/mL Recombinant Human IL-4 (Miltenyi Biotec) for 7 days at 37°C with 5% CO_2. Fresh medium with cytokines, at concentrations stated above, was added on day 3. Mature DC were obtained by adding 1 mg/mL lipopolysaccharide at day 5 of differentiation.

DC-10 were generated as previously described.[17] Briefly, CD14$^+$ monocytes were cultured as described above for DC differentiation, with the addition of Recombinant Human IL-10 (CellGenix) at 10 ng/mL.

METHOD DETAILS

AHR and MTOR modulation
AHR pathway modulation was performed by adding the AHR agonist 2-(1'H-indole-3'-carbonyl)-thiazole-4-carboxylic acid methyl ester (ITE) (Invivogen) (30μM) or the synthetic AHR antagonist CH-223191 (Invivogen) (20μM, unless differently indicated) to the culture medium of differentiating CD14+ monocytes at day 0 (see cell preparation and DC differentiation paragraph above). MTOR activation was performed by adding MHY1485 (Calbiochem) (20μM or 50μM, as indicated) to the culture medium of differentiating

CD14+ monocytes at day 0 (see cell preparation and DC differentiation paragraph above). AHR agonist/antagonist and MTOR activator were replenished at day 3 of culturing.

Mixed lymphocyte reaction (MLR) assay

Total CD4$^+$ T cells were purified from PBMCs by negative selection using the human CD4$^+$ T cell Isolation Kit II (Miltenyi Biotec) according to the manufacturer's instructions. Naive CD4+ T cells were purified from total CD4+ T cells by negative selection with CD45RO microbeads (Miltenyi Biotec) according to the manufacturer's instructions.

Short term MLR

T cells were labeled with Cell Proliferation Dye eFluor450 (eBioscience) according to manufacturer's instructions and stimulated with allogeneic *in vitro* differentiated DC/DC-10 (10:1, T:DC ratio) in X-VIVO 15 medium (Lonza) supplemented with 5% human serum (Sigma Aldrich) and 100 U/mL penicillin/streptomycin (Lonza). When indicated, 20 μM CH-223191 was added. Unstimulated and anti-CD3/CD28 bead (T cell activator beads, Invitrogen) stimulated CD4$^+$ T cells were used as negative and positive controls, respectively, of proliferation. After 5 days of culture at 37°C and 5% CO$_2$, MLR supernatants were frozen for ELISA testing and cells were collected and stained. Phenotype and proliferation dye dilution were analyzed by flow cytometry (FC).

Long term MLR and II MLR

Unstained CD4$^+$ T cells were plated with DC/DC-10 as described for short term MLR. After 10 days, cells were counted and a fraction was stained for FC. Another fraction was stained by efluor450 proliferation dye and re-plated with mature DC (10:1, T:DC) derived from CD14$^+$ obtained from the same donor used in long term MLR. After 3 days, MLR supernatants were frozen for ELISA testing and cells were collected and stained. Phenotype and proliferation dye dilution were analyzed by FC.

Flow cytometry (FC) analysis

Unless otherwise specified, all stainings were performed for 10 min at room temperature in the dark in BD Brilliant Buffer (Becton Dickinson).

Only single (as assessed by forward side scatter - high (FSC-H) vs FSC-area (FSC-A) plot), living (live/dead^{low}) cells were considered in the analysis. Data were analyzed with FlowJo Software.

Relative fluorescence intensity (RFI) for a given staining was calculated as the ratio between MFI of the stained sample and MFI of the unstained sample.

In vitro DC/DC-10 phenotype: at the end of the differentiation, dead cells were stained by blue or orange live/dead staining (Life Technologies) according to manufacturer's instructions. After washing, cells were stained by cells were stained in Brilliant buffer containing fluorochrome-conjugated antibodies against the following surface molecules: CD1a, CD14, CD16, HLA-DR, CD11c, CD163 (Becton Dickinson), CD141 (Miltenyi Biotec), *CLEC4G* (R&D Systems), CD86 (Life Technologies), CD83, HLAG (MEM-G9), ILT4 (Beckman Coulter), PDL1 (eBioscience), and CD40 (Becton Dickinson), combined according to the staining panels shown below.

Fluorochrome	Mix 1	Mix 2	Mix 3	Mix 4	Mix 5
FITC	CD1a	CD1a	CD14	–	CD206
PE	HLA-G	PDL1	DC-SIGN	DC-SIGN	CD1A
PerCPCy5.5	CD86	CD163	CD163	CD14	CD14
PE-CF594	–	–	CD86	CD86	CD86
PE-Cy7	CD11c	CD11c	CD11c	CD11C	CD11C
APC	ILT-4	CLEG4G	HLA-G	HLAG	ILT-4
APC-H7	CD14	CD14	HLA-DR	HLADR	–
Pacific Blue/BV421	CD163	CD16	CD16	CD163	CD163
Brilliant Violet 510	CD16	HLA-DR	–	CD16	CD16
Brilliant Violet 711	CD141	CD141	CD141	CD141	CD141
Brilliant Violet 786	CD83	–	–	–	–
BUV737	–	–	CD83	CD83	–

Samples were analyzed by LSR Fortessa and FACSymphony Flow Cytometers (BD Biosciences).

The hierarchical clustering heatmap was obtained via Morpheus (https://software.broadinstitute.org/morpheus/) by using one minus Spearman rank correlation and average as the linkage method. We used, as input parameters, the percentage of positive cells for CD14, CD16, CD141, CD163, CLEGC4-G, ILT-4, HLA-G, PD-L1, CD86, CD83, HLA-DR in 19 DC-10 and 19 DC-10 CH223191 differentiated samples.

MLR experiments: dead cells were stained with near-infrared viability dye according to manufacturer's instructions (live/dead staining, Miltenyi Biotec). The staining mix in PBS +2% FBS contained the following fluorochrome-conjugated antibodies: PE-Cy7

anti-CD11c, PE anti-CD25, BV510 anti-HLA-DR, PerCP-Cy5.5 anti-CD45RO and APC anti-CD4 (short term MLR). Long-term MLR cells were stained at 37°C for 15 min with PE anti-LAG3, PerCP-Cy5.5 anti-CD45RO, PE-Cy7 anti-CD4, APC anti-CD49b, BV421 anti-CD25 and BV510 anti-HLA-DR as previously described,[33] followed by intra-cellular FITC anti-Ki67 staining using Fix/Perm staining buffers (eBiosciences) following manufacturer's instructions.

II MLR cells were stained with FITC anti-CD45RA, PE anti-HLA-DR, PerCP-Cy5.5 anti-CD45RO, PE-Cy7 anti-CD4 and APC anti-CD25 in PBS +2% FBS.

Samples were analyzed using a FACSCanto II cell analyzer (BD Biosciences).

Ex vivo DC-10 staining: 180μL of whole blood were incubated with each of the following antibodies: FITC anti-CD11C, PE anti-HLA-G, PerCP-Cy5.5 anti-CD163, PC7 anti-CD83, APC anti-ILT4, APC-H7 anti-CD14, PB anti-CD141 and BV510 anti-CD16 for 15 min at room temperature in the dark. Red blood cells were then lysed by Ammonium Chloride buffer.

Samples were analyzed using a FACSCanto II cell analyzer (BD Biosciences).

STAT3 phosphorylation assay: differentiating dendritic cells were harvested at 2 and 5 days of differentiation, washed and seeded in a new plate, where they were exposed or not to IL-10 (10 ng/ml). After 30 min of incubation, cells were fixed by formaldehyde, permeabilized by methanol and stained by phospho-STAT3 antibody (PY705, BD Phosflow). For each condition, phosphorylation level is expressed as the ratio between MFI of IL-10 exposed cells and MFI of not exposed cells. Samples were analyzed using a FACSCanto II cell analyzer (BD Biosciences).

Ribosomal protein S6 phosphorylation assay: differentiated dendritic cells were harvested at 2 days of differentiation and seeded in a new plate, where they were exposed to IL-10 (10 ng/ml) with or without MHY1485 (20μM or 50μM). After 30 min of incubation, cells were fixed by formaldehyde, permeabilized by methanol and stained by Phospho-S6 (Ser235, Ser236) Monoclonal Antibody (cupk43k, Thermo Scientific). For each condition, phosphorylation level is expressed as the ratio between MFI of stained cells and MFI of not stained cells. Samples were analyzed using a FACSCanto II cell analyzer (BD Biosciences).

Cytokine production by ELISA
MLR supernatants were tested without dilution by standard ELISA. Below the list of reagents used.

Coating Ab	Clone	Brand	Concentration
Purified Rat Anti-Human and Viral IL-10	JES3-9D7	BD Biosciences	1 μg/mL
Purified Mouse Anti-Human IFNg	NIB42	BD Biosciences	1 μg/mL
Detection Ab	**Clone**	**Brand**	**Concentration**
Biotin Anti-Human and Viral IL-10	JES3-12G8	BD Biosciences	1 μg/mL
Biotin Anti-Human IFNg	4S.B3	BD Biosciences	1 μg/mL
Standard Curve		**Brand**	**Concentration (max:min)**
Recombinant Human IL-10 protein	–	CellGenix	2000 : 15,625 pg/mL
Recombinant Human IFNg	–	R&D Systems	2000 : 15,625 pg/mL

Quantification of signal was performed using Streptavidin covalently coupled to horseradish peroxidase (strep-POD) and Tetramethylbenzidine (TMB) substrate, and optical density (OD) was read at 640nm on a Multiskan GO (Thermo Fisher Scientific) and analyzed by SkanIt 4.1. Absolute concentration of each cytokine was quantified by plotting sample OD on a standard curve loaded in duplicate on each plate and obtained by 2-fold serial dilutions.

Cell sorting
Peripheral blood mononuclear cells or monocyte-enriched mononuclear cells (obtained as described in[18]) were sorted on a FACSAria Fusion Cell Sorter after staining with:

FITC anti-CD1c, PE anti-CD141, PerCP-Cy5.5 anti-CD14, PE-Cy7 anti-CD11c and Alexa 647 anti-CD16 (for evDC-10/cDC isolation used for ATAC-seq; see Figure S6 for gating strategy); Zombie Green, PE anti-CD141, PerCP-Cy5.5 anti-CD14, PE-Cy7 anti-CD11c and Alexa 647 anti-CD16 (for isolation of DC-10 and monocytes from HC/MS donors).

Cells were collected in a cold block under sterile conditions.

Gene expression analysis by droplet digital PCR (dd-PCR)
Total RNA was extracted using RNeasy Kit (QIAGEN) according to the manufacturer's instructions and quantified using Fluorometer Qubit with Qubit RNA HS Assay Kit (ThermoFisher).

cDNA was synthesized by High-capacity cDNA Reverse Transcription Kit (Applied Biosystems), according to the manufacturer's instructions, and 1-2ng of RNA equivalent were run per well of ddPCR. Amplification of target genes was performed using either QX200 ddPCR EvaGreen Supermix (Bio-Rad) and specific primers designed for test targets and house-keeping control (HPRT),

or with purchased probe-based systems and ddPCR Supermix for Probes (Bio-Rad). Below the list and sequences of home designed primers.

Target gene	Chemistry	Forward primer sequence	Reverse primer sequence
AHRR	EvaGreen	GACATGAAGCTGCAAGGTG	TGGACACATCTAGCAGCAG
CYP1B1	EvaGreen	AAGACAGTGGAGATGAGGG	CTGTCATCTGTGAGTGTGG
HPRT	EvaGreen	CAAAGATGGTCAAGGTCGC	CAAATCCAACAAAGTCTGGCT
IRF1	EvaGreen	CTCTGAAGCTACAACAGATGAG	GTAGACTCAGCCCAATATCCC
DDIT4	EvaGreen	TTAGCAGTTCTCGCTGACC	CTAGGCATGGTGAGGACAG

Purchased system are provided in the key resources table.

Droplets were generated by a QX200 Droplet Generator (Bio-Rad) and transferred into a 96-well plate for PCR amplification. PCR amplification was performed on a T100 Thermal Cycler (Bio-Rad) and fluorescence was read by QX200 Droplet Reader (Bio-Rad). Data were analyzed by QuantaSoft software (Biorad). Expression of a test gene was quantified by normalizing the number of positive droplets per μl of the test gene divided by the number of positive droplets per μl of HPRT in the same sample.

RNA-seq and microarray

RNA was extracted with an miRNeasy Kit (Qiagen) following manufacturer's instructions. After QC by Qubit (ThermoFisher) and TapeStation (Agilent), libraries based on rRNA depletion or polyA-selection (only for MS samples) were built and sequenced by 2x150 Illumina HiSeq 2000 or NovaSeq 6000.

Raw RNA sequences were aligned against the human reference genome GRChg19 using STAR (v 2.7.5a). FeatureCounts (v. 2.0.1) was used to determine the total counts of transcripts per gene. Differential gene expression and clustering were performed in the R statistical environment using the DESeq2 package. Gene set enrichment analyses were performed by Enrichr (https://maayanlab.cloud/Enrichr/)[85] and Metascape (metascape.org)[86] by using default settings and DEG (adjusted p < 0.01) genes as input lists.

We have previously published RNA-seq of *ex vivo* DC-10 and cDC (GSE117945).[18] We have used a published microarray dataset of IL-10 stimulated and unstimulated monocytes (GSE82316)[87] and re-analyzed published RNA-seq data from MS and HC monocytes (GSE137143), using only CD14+_RRMS and CD14+_Healthy samples.

ATAC-seq

Library preparation was performed on 0.5-1x10^5 cells by Tagment DNA enzyme and buffer Small kit (Illumina), as previously described,[88] with minor modifications, and sequenced by 2x150 Illumina HiSeq.

Paired-end FASTQ reads were trimmed with trimmomatic (v 0.36) using the Nextera adapter library. Trimmed reads were then mapped on the hg19 version of the human genome using bwa-mem with default settings and duplicates were marked using samblaster (v 0.1.21). Duplicates, blacklisted regions (ENCODE) and reads aligning with mitochondrial DNA were removed using samtools (v 0.1.19). Broad peaks were called using MACS2 (v. 2.1.1; –shift −100 –extsize 200 –broad). The list of called peaks from each sample was used to assess the differentially open chromatin regions through the DiffBind package from the R statistical environment using edgeR and DESeq2 methods (FDR<0.01 and FC > 2 for *in vitro* data, FC > 4 for *ex vivo* data, where fold change values were larger). Matching results obtained by the two methods were used to define the list of differentially accessible regions that were in common across both DC-10 and DC. In case of groups with less than 3 samples (AHRinhDC-10 experiment) or more than 3 samples (*ex vivo* DC-10 experiment), only EdgeR or DESeq2 results were considered, respectively.

ChIP-seq

Chromatin immunoprecipitation was performed on 2–4 million cells, as previously described,[89] by using rabbit polyclonal anti-H3K27ac, H3K4me1 and H3K9me3 antibodies (all from Abcam).

Paired-end FASTQ reads were trimmed with trimmomatic (v 0.36) using the Nextera adapter library. Trimmed reads were then mapped on the hg19 version of the human genome using bwa-mem with default settings and duplicates were marked using samblaster (v 0.1.21). Duplicates, blacklisted regions (ENCODE) and reads aligning with mitochondrial DNA were removed using samtools (v 0.1.19). Broad peaks were called using MACS2 (v. 2.1.1; –shift −100 –extsize 200 –broad).

Enhancer identification and annotation

In order to identify accessible robust enhancers, the list of differentially accessible regions was filtered using the list of human 'robust' enhancers from the FANTOM5 project (http://slidebase.binf.ku.dk/human_enhancers/presets - section 1), and the Enhancer - Promoter association matrix made for decomposition-based peak identification clusters (http://slidebase.binf.ku.dk/human_enhancers/presets - section 5) was used to infer the putative target genes of the previously identified enhancers.

To test whether the *in vitro* identified DC-10-specific robust enhancers tend to be AHR-dependent *in vitro* and *ex vivo* DC-10-specific, we performed Fisher's exact test (FDR<0.01) on 2 x 2 tables, organized as follows:

For AHR dependency (Figure 5B).

# DC-10 robust enhancers in DC-10 peaks (log2FC > 0 in volcano)	# DC-10 robust enhancers in AHRinhDC-10 peaks (log2FC < 0 in volcano)
# DC-10 peaks (log2FC > 0 in volcano)	# AHRinhDC-10 peaks log2FC < 0 in volcano)

For *ex vivo* DC-10 (Figure 6A).

# DC-10 robust enhancers in evDC-10 peaks (log2FC > 0 in volcano)	# DC-10 robust enhancers in cDC peaks (log2FC < 0 in volcano)
# evDC-10 peaks (log2FC > 0 in volcano)	# cDC peaks (log2FC < 0 in volcano)

Transcription factor motif identification

In order to identify potential transcription factors involved in the biology of *in vitro* differentiated DC-10, the 'peak-motif' tool from Regulatory Sequence Analysis Tools (RSAT) (http://rsat.sb-roscoff.fr/)[90] was used.

For each condition, we used the FASTA sequences of the identified enhancer as the test and a universe of all the peaks found in the experiment as the background control.

The same approach was used for the promoters of putative target genes. We inferred the promoter region of each gene by adding +/−1 kb to the TSS. The entire list of promoters from the hg19 genome was used as the background control (UCSC).

The analysis was run by using default settings and interrogating the JASPAR, ENCODE and HOCOMOCO databases to correlate the motifs identified as enriched with potential TF binding sites. The list of TFs was obtained by merging the results from each database. Word clouds were obtained using Wordart (wordart.com) by assigning to each TF an enrichment score, based on the enrichment of the found motif, normalized correlation between motif and binding site, and number of found motifs correlating with the binding site in the ENCODE database.

TFmotifView (http://bardet.u-strasbg.fr/tfmotifview/)[47] was used to assess the enrichment of selected TF binding sites in enhancers and promoter sequences (obtained as described above) of *in vitro* and *ex vivo* DC-10. Analysis was performed using default settings.

Transcription factor network

The STRING (v11) (https://string-db.org) protein-protein network tool was employed[26] to identify potential interactions among transcription factors. Networks were built with a minimum required interaction score of 0.4, and only connected nodes are shown. To validate the significance of the analysis in Figure 1F, we simulated the PPI network 1000 times using randomly selected TFs from the entire list of human TFs (same number as DC-10 TF).

Feature alignment

Specific enhancer datasets were intersected with H3K9me3, H3K27ac and H3K4me1 ChIP-Seq data. The deepTools2 server, and in particular the modules *computeMatrix* and *plotProfile,* were used to scale (—scale-regions), align all the features and plot the results.

Gene set enrichment analysis (GSEA)

GSEA (https://www.gsea-msigdb.org/gsea/index.jsp)[91] was used to assess whether a defined set of genes showed statistically significant, concordant differences in term of expression between two groups of a sample. Standard parameters with gene set permutation type were used for the analysis and differences were considered significant with FDR<0.25. Gene sets used in this work are listed in Table S3.

QUANTIFICATION AND STATISTICAL ANALYSIS

Because assumptions for the correct application of parametric tests were not met or not verifiable, statistical analyses for significant differences were performed with non-parametric tests: Wilcoxon matched pairs signed rank test when comparing two groups, Kruskal-Wallis test followed by Dunn's multiple comparison test when comparing more than two groups and Mixed effect model with Geisser-Greenhouse correction followed by Sidak's multiple comparison test, when comparing more than two groups with

multiple variables. Differences were regarded as significant at p values <0.05, only significant p values are reported in figures. Statistical tests used and number of biological replicates (n) are reported in the figure legends. Values are expressed as medians and interquartile ranges in box/scatter/violin plot graphs. The results were analyzed using GraphPad Prism v9.0 and v10 (GraphPad Software).

FDR reported in Figure 2A are obtained by Deseq2 analysis of RNA-seq data, FDR is reported as 0 when below 2.225074e-308.
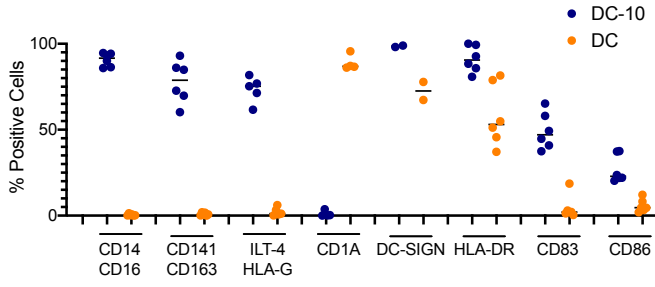
Supplemental information

Aryl hydrocarbon receptor activity downstream

of IL-10 signaling is required to promote

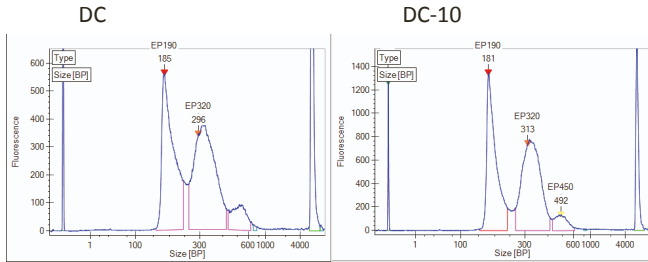# regulatory functions in human dendritic cells

Daniele Avancini, Alessandro Testori, Lucia Fresolone, Grazia Andolfi, Michela Vuono, Vittorio Martinelli, Francesca R. Santoni de Sio, and Silvia Gregori
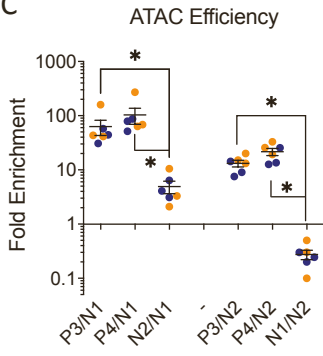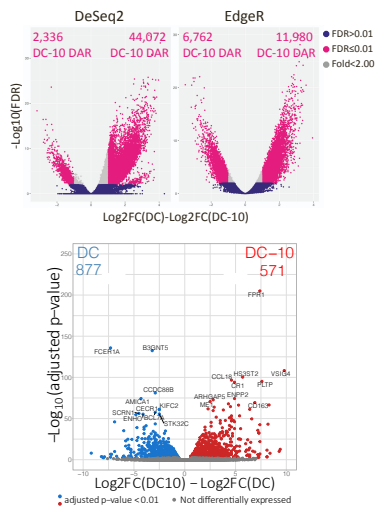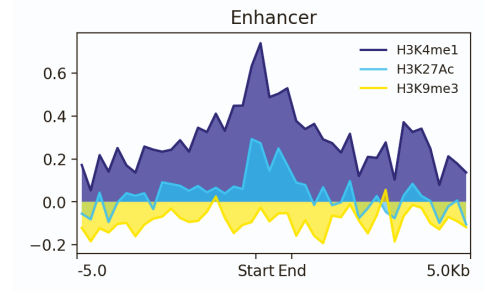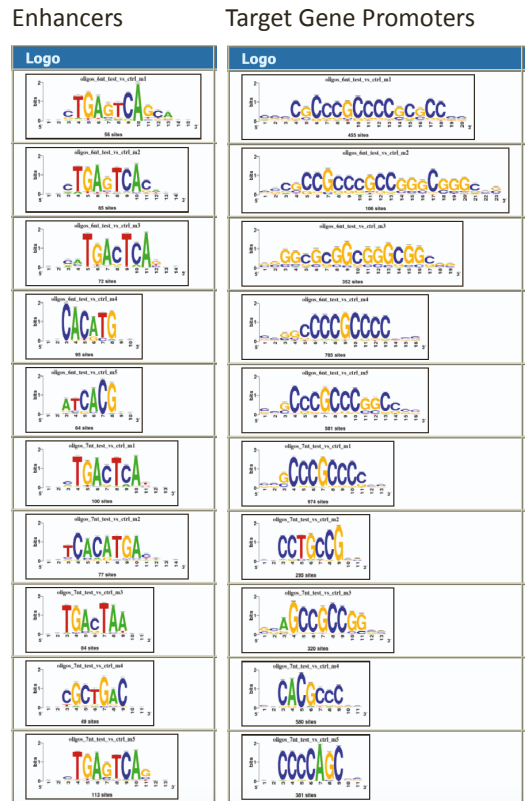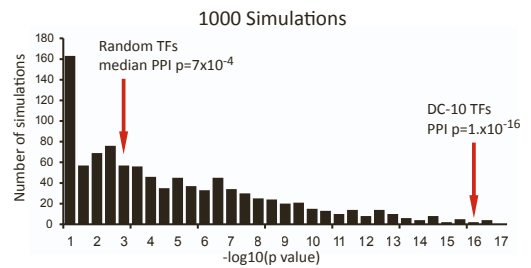
Figure S1

Figure S1. Relative to Figure 1 *IL-10 Impacts Chromatin and Transcription in DCs*

A) Flow Cytometry profile of DC-10 (blue) and DC (orange) samples used for ATAC- and RNA-seq (n=6). Percentage of cells positive for indicated markers is shown.

B-C) ATAC Efficiency of tagmentation (B) and enrichment of accessible genomic sites (C) in DC-10 (blue) and DC (orange) samples. B) Electropherograms of purified ATAC libraries showing DNA sizes corresponding to 1-, 2- and 3-nucleosome stretches for DC and DC-10 samples. C) Droplet Digital PCR analysis with primers amplifying accessible (P3, P4) or non-accessible (N1, N2) regions in hematopoietic cells (Grbesa et al. 2017, *Journal of Visualized Experiments*, https://doi.org/10.3791/56313). Fold enrichment is expressed as the ratio between positive and negative signals (number of positive molecules *per* mL in accessible regions/number of positive molecules *per* mL in non-accessible regions) normalized to the average of the ratios between negative and negative signals (number of positive molecules *per* mL in non-accessible regions/number of positive molecules *per* mL in non-accessible regions; set as 1). *p*-values by Wilcoxon matched pairs test.

D) ATAC-seq (top) and RNA-seq (bottom) volcano plots of DC-10 vs. DC samples. Top plots display differentially accessible genomic regions (DAR) (pink) by DESeq2 and edgeR algorithms. Bottom, differentially expressed genes (DEG) (red) by DESeq2 with top 10 DEG name per group indicated. The number of DAR and DEG per group are indicated.

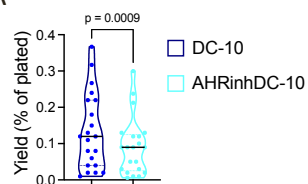E) Feature alignment of ChIP-seq results obtained for the 3 indicated histone marks in DC-10 on the 107 DC-10 enhancers (start-end of the sequences are indicated).

F) Motif logos of the 10 most enriched motifs in enhancer and target gene promoter regions found using the RSAT tool.

G) PPI *p*-values obtained by the STRING tool in 1000 simulations performed with TFs randomly chosen from the ENCODE human TF list.

Figure S2

A

p = 0.0009

Yield (% of plated)

□ DC-10
□ AHRinhDC-10

B

DC-10

| 28,4 | 65,5 |
| 5,16 | 0,94 |

| 15,0 | 62,8 |
| 7,91 | 14,2 |

| 51,4 | 43,6 |
| 3,88 | 1,17 |

| 9,38 | 29,3 |
| 29,4 | 31,9 |

| 35,7 | 48,4 |
| 13,5 | 2,48 |

unstained

AHRinh DC-10

| 4,16 | 3,92 |
| 81,6 | 10,3 |

| 51,7 | 1,47 |
| 46,7 | 0,18 |

| 9,22 | 2,07 |
| 85,8 | 2,88 |

| 4,16 | 2,87 |
| 83,4 | 9,57 |

| 9,02 | 32,6 |
| 23,0 | 35,4 |

CD14 / CD16
CD141 / CD163
CLEG4G / PD-L1
HLAG / ILT-4
CD83 / CD86
Normalized Count / HLA-DR

C

DC-SIGN   CD1A   CD206

% positive cells

p=0.0010
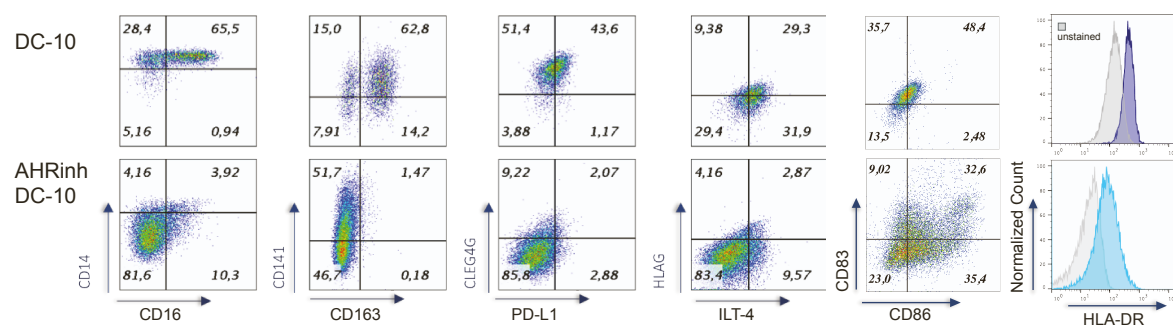
■ DC-10
□ AHRinhDC-10
□ DC

Figure S2. Relative to Figure 2 *AHR activity characterizes IL-10 induced tolDC*

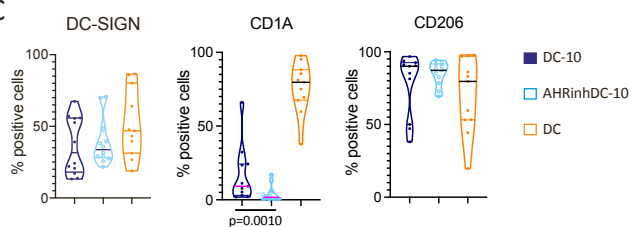CD14$^+$ monocytes isolated from peripheral blood (PB) were differentiated *in vitro* for 7 days in the presence of GM-CSF, IL-4 and IL-10 with (AHRinhDC-10) or without (DC-10) the AHR inhibitor (AHRinh) CH223191 (20μM).

A) Cell yield upon 7 days of DC-10 (blue) and AHRinhDC-10 (light blue) differentiation. Yield is expressed as number of recovered cells/number of plated cells (n=21).
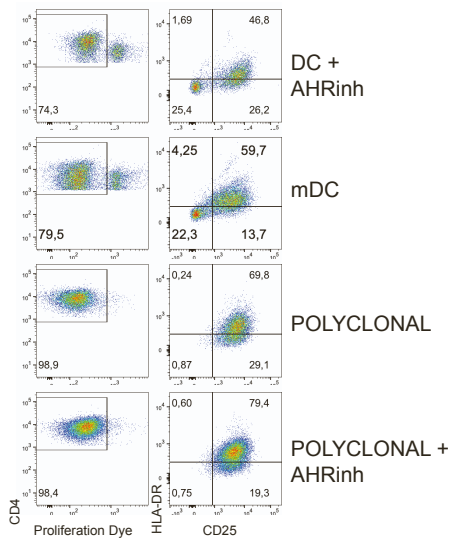
B) Representative flow cytometric plots showing the expression of the indicated markers in DC-10 (top) and AHRinhDC-10 (bottom).

C) Percentage of DC-10 (blue), AHRinhDC-10 (light blue) and DC (orange) expressing the DC differentiation markers DC-SIGN (CD209), CD1a and CD206 analyzed by flow cytometry (n=11-12).
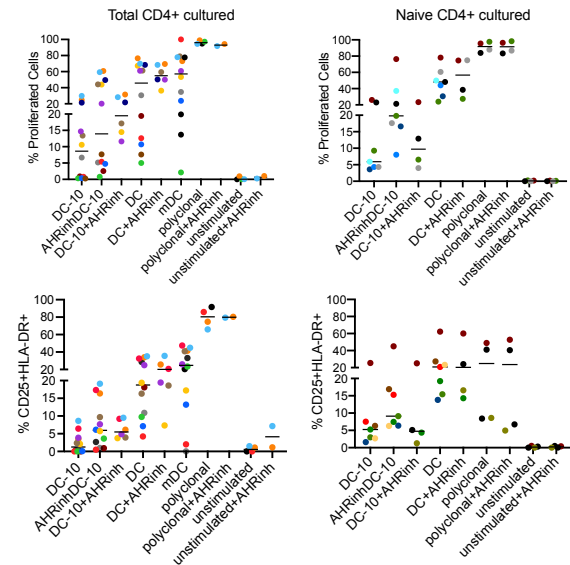
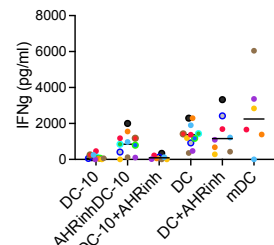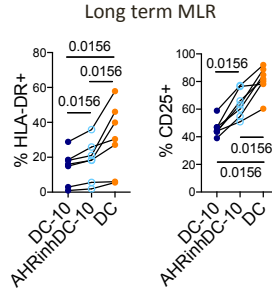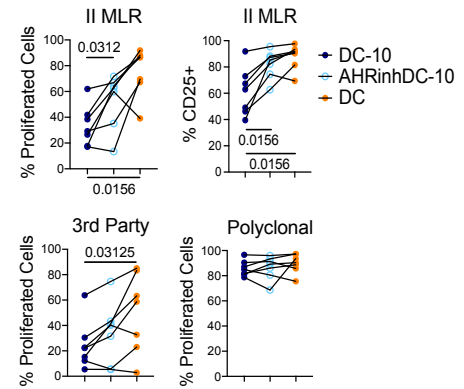p values by Wilcoxon matched pairs test.

Figure S3

Figure S3. Relative to Figure 3 *AHR activation is necessary for IL-10 induced tolerogenic functions in tolDCs generated in vitro*

A-C) Short-term MLR. Allogeneic CD4$^+$ T cells were stimulated *in vitro* with the indicated DC. After 5 days, T cell proliferation and activation were tested by flow cytometry and IFNg production in culture supernatants was tested by ELISA.

A) Representative flow cytometric plots showing the expression of the indicated markers in CD4$^+$ T cells stimulated with DC in the presence of the AHR inhibitor CH223191 (20μM), mDC or with anti-CD3/anti-CD28 coated beads (Polyclonal) in the absence or presence of AHR inhibitor CH223191 (20μM).

B) Raw percentages of proliferating (top) and CD25$^+$HLA-DR$^+$ (bottom) CD4$^+$ cells in MLR of total (left) and naïve (right) CD4$^+$ cells stimulated by the indicated DC. Each color represents an independent donor, line at median.

C) IFNg ELISA quantification in culture supernatants of T cells stimulated by the indicated DC. Each color represents an independent donor, line at median.

D-E) Long-term MLR and II MLR. Long-term MLR: allogeneic CD4$^+$ T cells were stimulated by the indicated DC. The percentage of proliferating and Tr1 cells was assessed after 10 days by flow cytometry. II MLR: CD4$^+$ T cells primed in I MLR by the indicated DC were re-stimulated with mature DC derived from the same donor used in I MLR. After 3 days of re-stimulation, proliferation by flow cytometry and cytokine production by ELISA on culture supernatants were assessed.

D) Raw percentages of CD25$^+$ and HLA-DR$^+$ cells in I long-term MLR of T cells stimulated with the indicated DC.

E) Top, raw percentages of proliferating (left) and CD25$^+$ (right) CD4$^+$ cells after II MLR. Bottom, percentage of proliferating CD4$^+$ upon stimulation with third party donor mature DC (left) and polyclonal stimulation by anti-CD3/anti-CD28 coated beads (right). Blue dots = T cells stimulated in I MLR by DC-10; light blue dots = T cells stimulated in I MLR by AHRinhDC-10; orange dots = T cells stimulated in I MLR by DC.

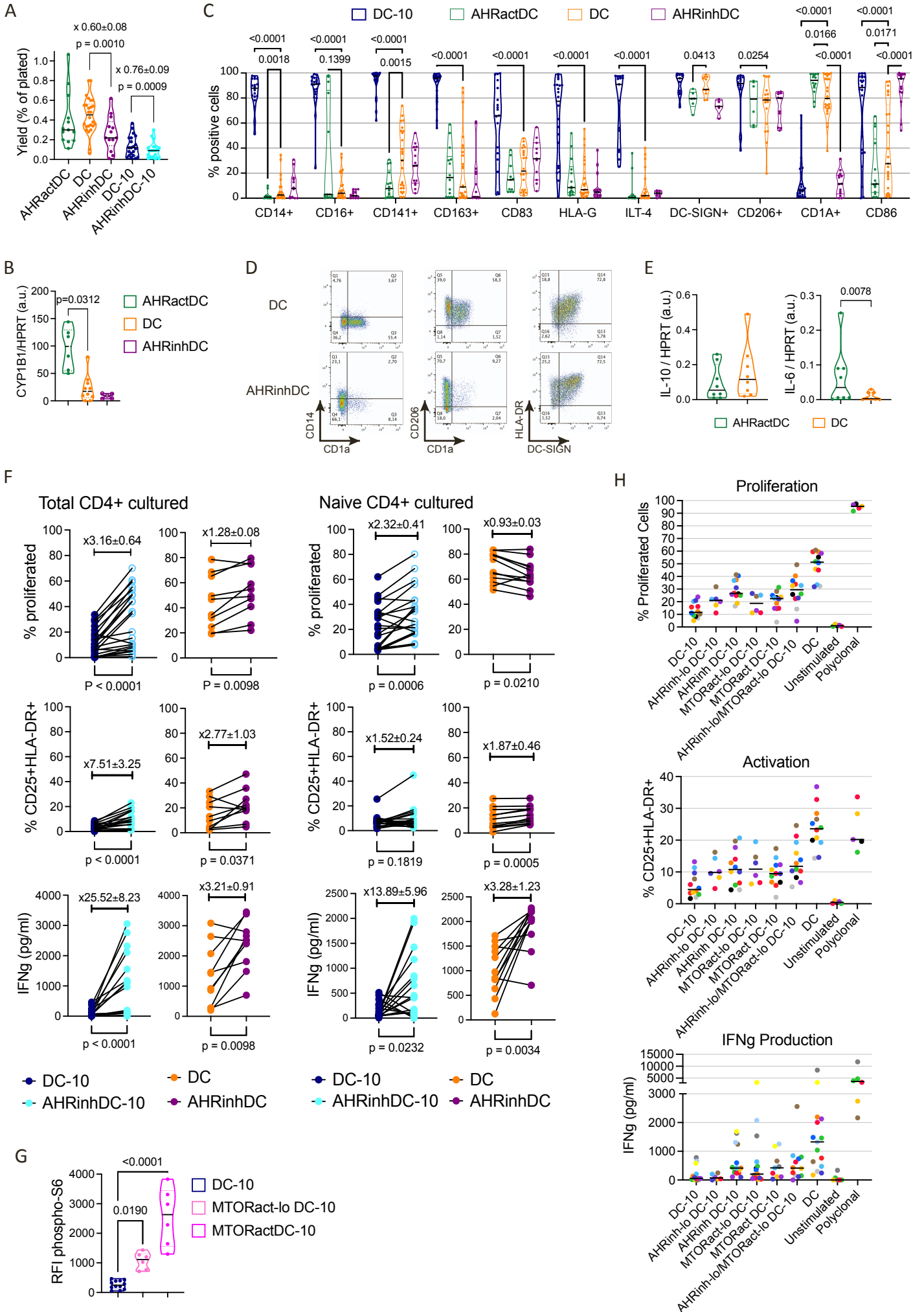*p*-values by Wilcoxon matched pairs test.

Figure S4

Figure S4. Relative to Figure 4 *AHR induced tolerogenic features are dependent on IL-10 and MTOR pathway inhibition*

CD14^{+} monocytes isolated from peripheral blood (PB) were differentiated *in vitro* for 7 days in the presence of GM-CSF, IL-4 and IL-10 (DC-10), GM-CSF and IL-4 without (DC) or with the AHR agonist ITE (30μM) (AHRactDC) or the AHR inhibitor CH223191 (20μM) (AHRinhDC).

A) Cell yield upon 7 days of AHRactDC (green), DC (orange) and AHRinhDC-10 (plum) differentiation. Yield is expressed as number of recovered cells/number of plated cells. To allow direct comparison, yield of DC-10 (blue) and AHRinhDC-10 (light blue), already shown in Fig. S2A, are reported. *p*-values by Wilcoxon matched pairs test and mean fold change±SEM are indicated.

B) Expression of the CYP1B1 gene in AHRactDC (green), DC (orange) and AHRinhDC (plum) by ddPCR. The ratio of molecules per μL amplified by CYP1B1 primers / molecules per μL amplified by HPRT primers is shown in arbitrary units (n=6-10). *p*-values by Wilcoxon matched pairs test.

C) Violin plots displaying the median +/- interquartile range of the percentage of positive cells expressing the indicated marker by flow cytometry in AHRactDC (green), DC (orange) and AHRactDC (plum) at 7 days of differentiation (n=11-25). p values by Mixed effect model with Geisser-Greenhouse correction followed by Sidak's multiple comparison test (comparing each group against DC).

D) Representative flow cytometry plots showing the expression of the indicated markers in DC (top panels) and AHRinhDC (bottom panels).

E) Expression of the IL-10 (top) and IL-6 (bottom) gene in AHRactDC (green) and DC (orange) by ddPCR. The ratio of molecules per μL amplified by IL-10 or IL-6 primers / molecules per μL amplified by HPRT primers is shown in arbitrary units (n=8). *P*-values by Wilcoxon matched pairs test.

F) Side-by-side comparison of T cell proliferation, activation and IFNg production obtained in short term MLR assays by stimulating T cells with DC-10 (blue) vs AHRinhDC-10 (light blue) (n=16-22) and DC (orange) vs AHRinhDC (plum) (n=10-12). Results after co-culture of total (left panels) and naive (right panels). Percentages of proliferating (top) and CD25^{+}HLA-DR^{+} activated (middle) CD4+ cells, assessed by flow cytometry; IFNg production (bottom), assessed in the culture supernatant by ELISA. *p*-values by Wilcoxon matched pairs test and mean fold change±SEM are indicated.

G) Phosphorylated-S6 (phospho-S6) fluorescence intensity (RFI, relative to unstained) DC-10 (blue), MTORact-lo DC-10 (pink) and MTORactDC-10 (magenta), assessed by flow cytometry at day 2 of differentiation. P values by Kruskal-Wallis test followed by Dunn's multiple comparison test (n=6-12).

H) Raw percentages of proliferating (top) and CD25^{+}HLA-DR^{+} (middle) CD4^{+} cells, and IFNg quantification in culture supernatants (bottom) in MLR of CD4^{+} cells stimulated by the indicated stimulus. Each color represents an independent donor, line at median.

Figure S5

A

Promoter Overlapping

3.680e-043

Number of Peaks

10000
1000
10
1

35 / 1594   695 / 5505

DC10-DC   DC10-AHRinhDC10

B

AHR-dependent Genes (Downreg. in AHRinhDC-10)
EnrichR - TF Perturbations Followed by Expression

MAF_siRNA_huMfage_down
p=2.07e-44

MAF_OE_huMfage_up
p=3.68e-28

LIN28_OE_huCD34_down
p=7.81e-27

-log10(p value)

Odds Ratio

C

AHR-dependent Genes (Downregulated in AHRinhDC-10)

NFE2L2 (CheA)
p=1.25e-13

STAT3 (ENCODE)
p=5.39e-13
STAT5a (ENCODE)
p=2.05e-12

-log10(p value)

EnrichR - ENCODE and ChEA Consensus TF targets Classes

D

Genes Upregulated in
AHRinhDC-10

● MCODE1: Leukocyte Activation
● MCODE2:
   Extracellular Matrix Organization
● MCODE3: SUMOylation

E

DC-10   AHRinhDC-10

Normalized Count

Phospho-STAT3

FMO
0
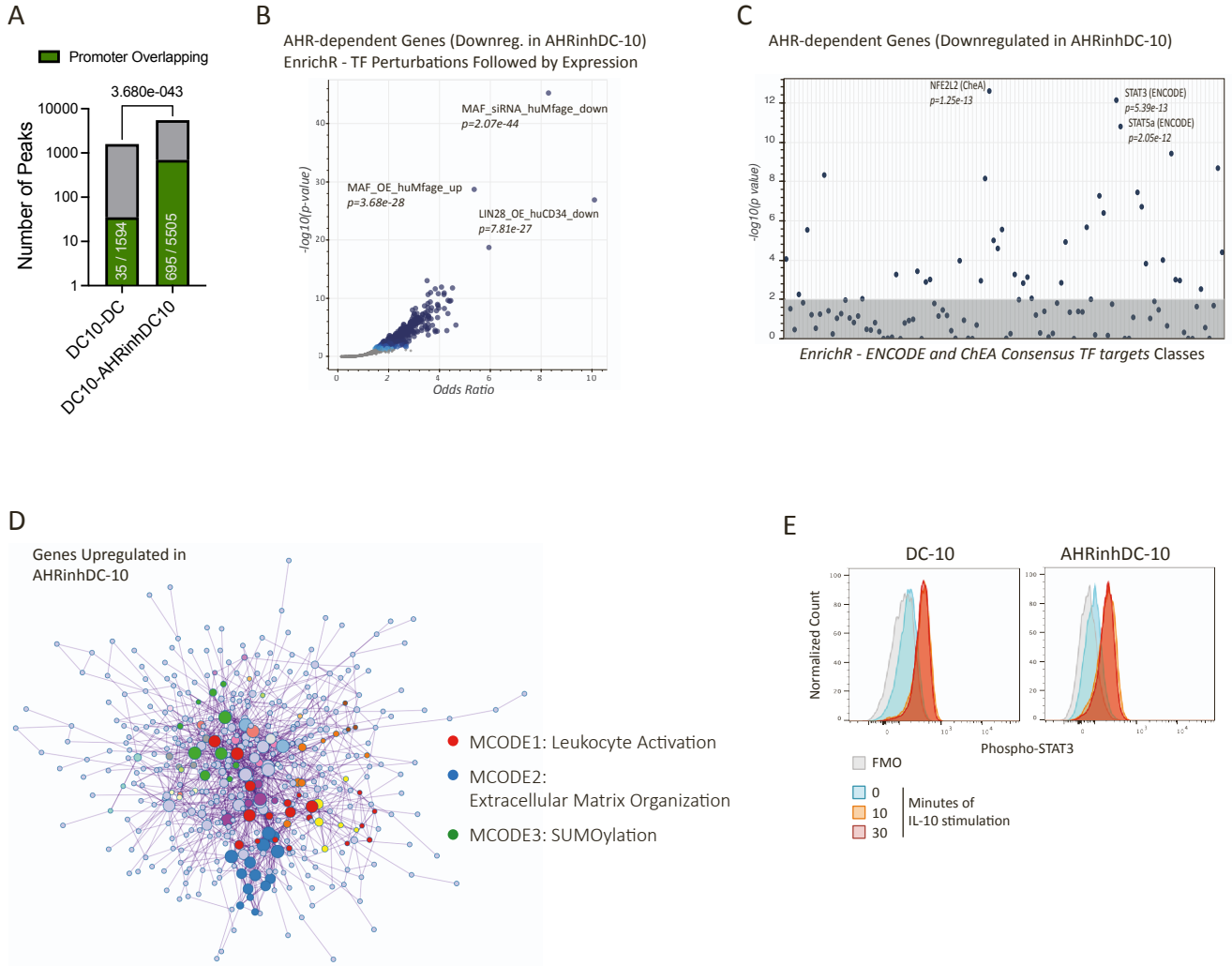10   Minutes of
30   IL-10 stimulation

Figure S5. Relative to Figure 5 *AHR activity controls IL-10-induced gene expression patterns*
A) Number of DC-10-specific peaks obtained from the comparison with DC (*in vitro* DC-10 vs. DC; DC10-DC) and AHRinhDC-10 (*in vitro* DC-10 vs. AHRinhDC-10; DC10-AHRinhDC10) (grey) and fraction of these peaks overlapping with mapped coding gene promoters (green bars). *p*-value by Fisher's exact test.

B, C) Enrichr gene enrichment analysis of genes downregulated in AHRinhDC-10 compared to DC-10. Top 3 classes with relative *p*-values are shown. B) Volcano plot of transcription factor perturbation followed by gene expression categories and C) Manhattan plot of ENCODE and ChEA transcription factor consensus target genes categories.

D) Gene enrichment analysis of genes upregulated in AHRinhDC-10 compared to DC-10: protein-protein interaction network components by MCODE Metascape algorithm. Top 3 MCODE component nodes are colored. MCODE1 (red) = GO:0002274 (myeloid leukocyte activation), GO:0002366 (leukocyte activation involved in immune response), GO:0002263 (cell activation involved in immune response); MCODE2 (blue) = R-HSA-1474244 (Extracellular matrix organization), R-HSA-1474290 (Collagen formation), R-HSA-1650814 (Collagen biosynthesis and modifying enzymes); MCODE3 (green) = R-HSA-3108232 (SUMO E3 ligases SUMOylate target proteins), R-HSA-2990846 (SUMOylation), R-HSA-3899300 (SUMOylation of transcription cofactors). GO = Gene Ontology; R-HSA = Reactome Gene Sets. GO categories associated to all MCODEs are described in Table S5.

E) Representative flow cytometry histograms of phospho-STAT3 analysis in DC-10 (left) and AHRinhDC-10 (right) incubated with IL-10 for the indicated times. Fluorescence minus one (FMO) signal is also shown.

Figure S6

A

DC-10 | cDC

B

evDC-10 ··· cDC

NES: 1.83 FDR=0.00

DC-10 Core Genes

C

BATF
MAF
BACH1
AHR

D

In Vitro DC-10

0.0286

● HC ● MS

% positive cells

CD14 CD16 CD141 CD163 CD83 CD86 HLA-DR HLA-G ILT-4

E

In Vitro DC-10

HC 0   MS 1

ULK4

Log2FC(MS) – Log2FC(HC)

● Not differentially expressed   ● adjusted p–value < 0.01

Ex Vivo DC-10

HC 0   MS 0

Log2FC(MS) – Log2FC(HC)

● Not differentially expressed (adjP>0.01)

F

-Log10(FDR)
● 0.60
● 2.32
● 9.00

Monocytes

NES

Demagalhaes_Aging Up
Fridman_Senescence Up
WP_Senescence and Autophagy in Cancer
Reactome_Oxidative Stress Induced Senecscence
Reactome_ Cellular Senenescence
WP_Kynurenine pathway and links to Cell Senescence
Reactome_Oncogene Induced Senescence
GOBP_Cell Aging
WP_NAD Metab. in Oncogene and Mitoc. Dysfunc.Senescence
Reactome_DNA Damage Telomere Stress Induced Senescence
GOBP_Multicellular Organism Aging

MS / HC

G

Ex Vivo DC-10

● HC ● MS
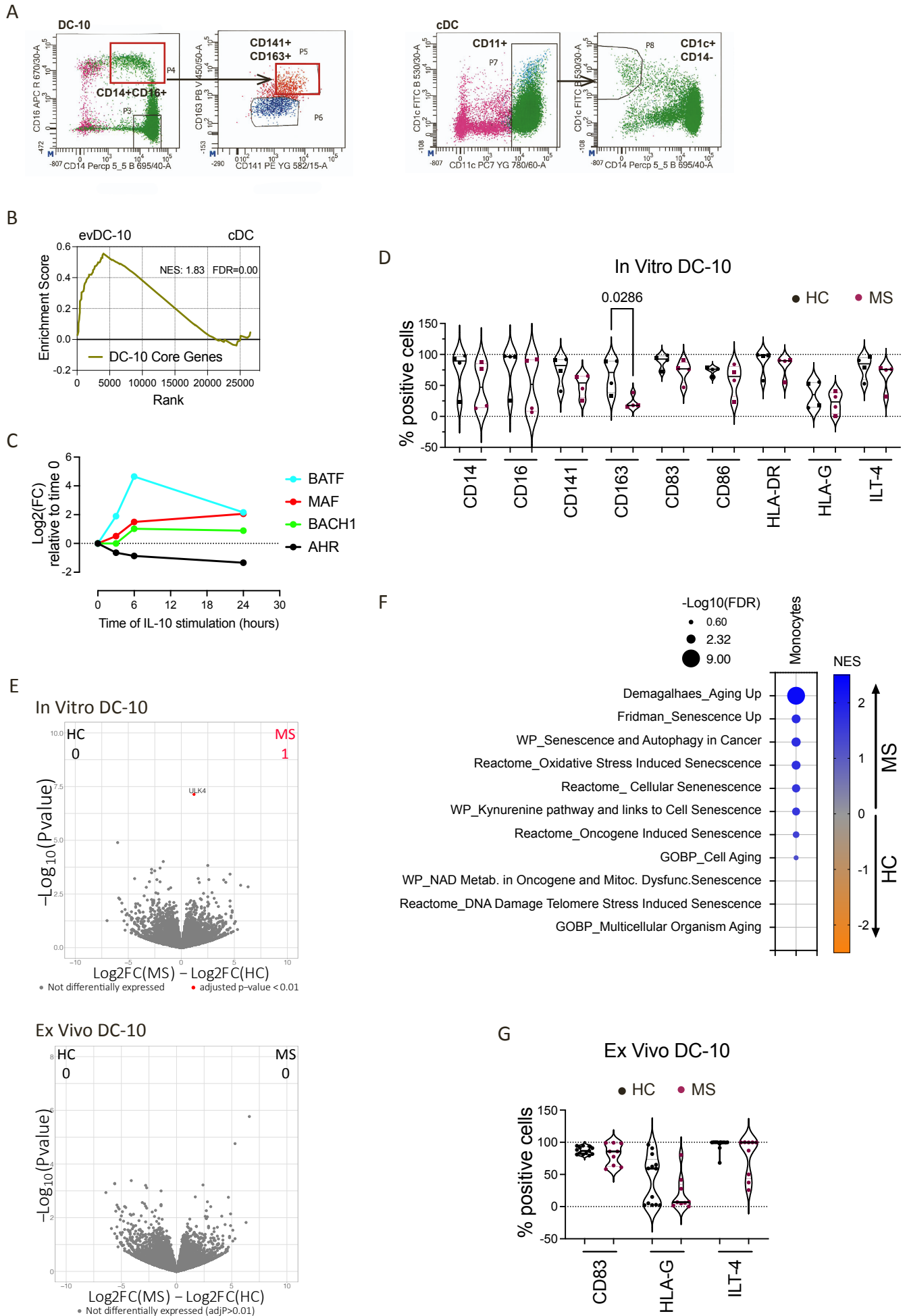
% positive cells

CD83 HLA-G ILT-4

Figure S6. Relative to Figure 6 *IL-10/AHR signature is active in vivo and is altered in autoimmune conditions*

A) Representative flow cytometry plots showing the sorting strategy for evDC-10 (left panels, red gates) and cDC (right panels) isolation from peripheral blood. Arrows represent sub-gating. Antibody and fluorochrome are shown on the axes.

B) GSEA of 91 DC-10 Core Genes (Table S1) in evDC-10 vs. cDC transcriptomes. Normalized enrichment score (NES) and FDR q value are reported. Leading-edge subset genes: 44.

C) Kinetic of expression upon IL-10 stimulation of the indicated transcription factors expressed as Log2 (Fold Change) versus time 0 monocytes (dotted line), assessed in Microarray data GSE82316.

D) Percentage of cells positive for the indicated markers in DC-10 differentiated from monocytes isolated from HC and MS donors (n=4). *p*-value by Mann-Whitney test.

E) RNA-seq volcano plots displaying differentially expressed genes (DEG) (red, adjusted p<0.01) by DESeq2, with top 10 DEG per group indicated, in MS vs. HC *in vitro* (top) and *ex vivo* (bottom) DC-10. The number of DEG in each group is indicated.

F) Normalized enrichment score (NES, color scale) and -Log10(FDR) (dot size) by GSEA of the indicated senescence-associated molecular signatures (see table S3) in the transcriptomes of MS and HC monocytes. FDR > 0.25 are not shown.

G) Percentage of circulating DC-10 expressing the indicated markers in healthy controls (HC) and multiple sclerosis (MS) donors by flow cytometry (n=9-13).